A Study of Pre-amorphization Formed by Plasma Doping Method

- A THESIS -

Submitted to Department of Advanced Applied Electronics, Interdisciplinary of Graduate School of Science and Engineering, Tokyo Institute of Technology, in partial satisfaction of the requirement for the degree of Master of Engineering.

Presented by:

04M36013 Issui Aiba

Supervisor:

Professor Hiroshi Iwai

Department of Advanced Applied Electronics
Interdisciplinary of Graduate School of Science and Engineering
Tokyo Institute of Technology

2006, February

Table of Contents

Chapter 1. General Introduction

1.1 Plasma Doping Method

1.1.1 Background

Nanotechnology has made a progress to satisfy with demand for such high performance personal computer and high frequency device. The downscaling of electronic devices have devoted to development of information technology and industry. In next generation, it is required to realize miniaturization of integrated circuits further.

This miniaturization is based on ‘the scaling rule’ downsized the device in both lateral and vertical direction. And the device parameters of next generation is provided in the International Technology Roadmap for Semiconductor(ITRS)[1].

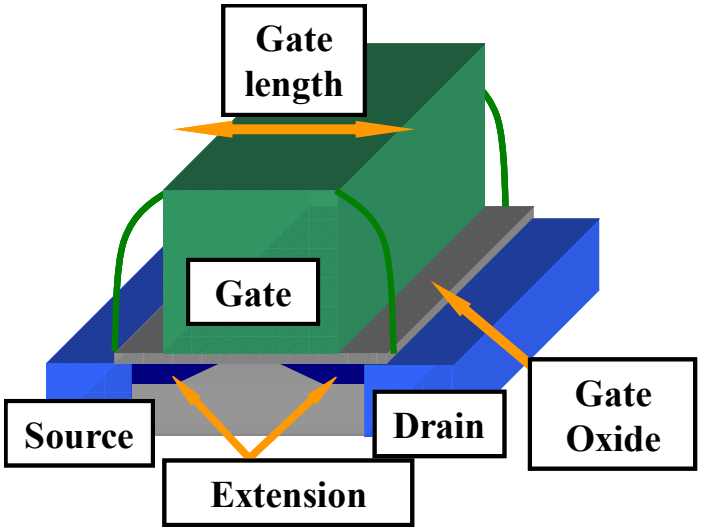

Fig.1 MOSFET schematic diagram

The future CMOS generations will require impurity doping techniques to realize ultra shallow junction as like less than 10nm. The realization of ultra shallow junction source and drain extension junction depths, that are vertically and laterally abrupt, requires not only the development of new and enhanced methods for implanting the doping species, but requires as well the development of thermal activation processes that have an extremely small thermal budget. Annealing technology is also required activate dopants efficiently and prevent from diffusion dopants. Fig.1 shows predicted Xj in the future by ITRS roadmap. Numerical targets of Xj is reduced proportional to year. Rs shows the characteristics tendency extremely. It is increased from 2005 to 2010, it is decreased after 2010. This tendency of Rs relates to development of annealing technology(Fig.2). According to ITRS roadmap, annealing time of nanosecond or microsecond order as such spike RTA, Flash ramp, Laser annealing will replace to Rapid thermal annealing(RTA). The current methods under investigation are identified in the potential solutions Figure3.

Year	2005	2006	2007	2008	2009	2010	2011
Rs[Ω/sq.]	767	833	884	1739	1800	1875	488
Xj[nm]	17.6	15.4	13.8	8.8	8	7.2	12.8

Year	2012	2013	2014	2015	2016	2017	2018
Rs[Ω/sq.]	518	514	557	550	549	547	536
Xj[nm]	11.2	10.4	8.8	8	7.2	6.4	5.6

Table.1 Rs and Xj in the future

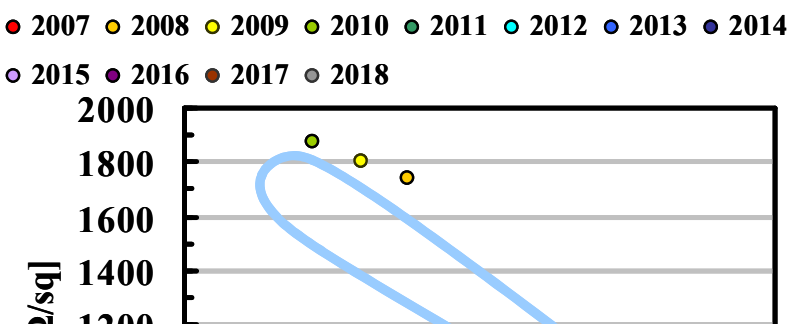

Fig.2 Requirement of Xj in the future(ITRS 2004updated)

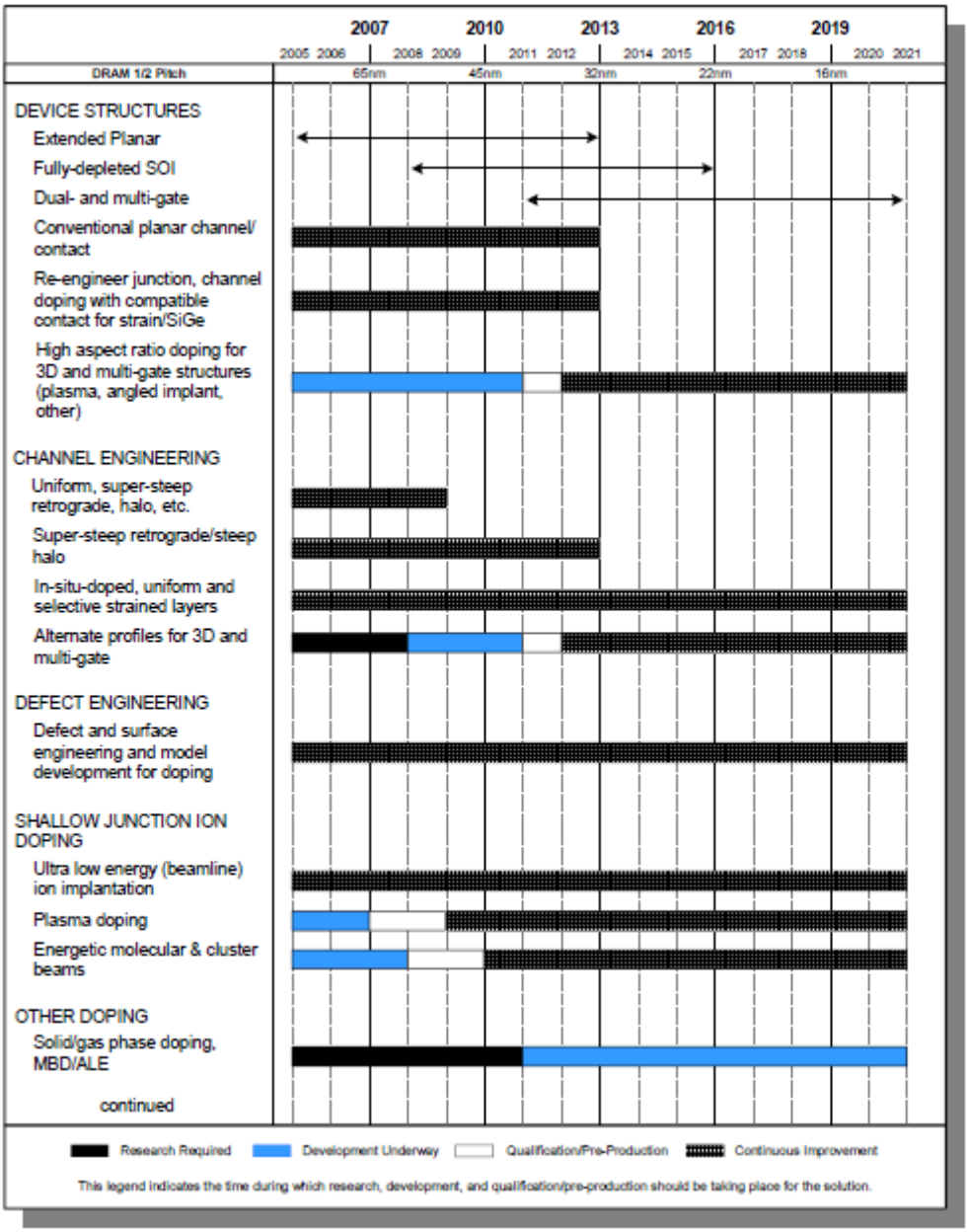

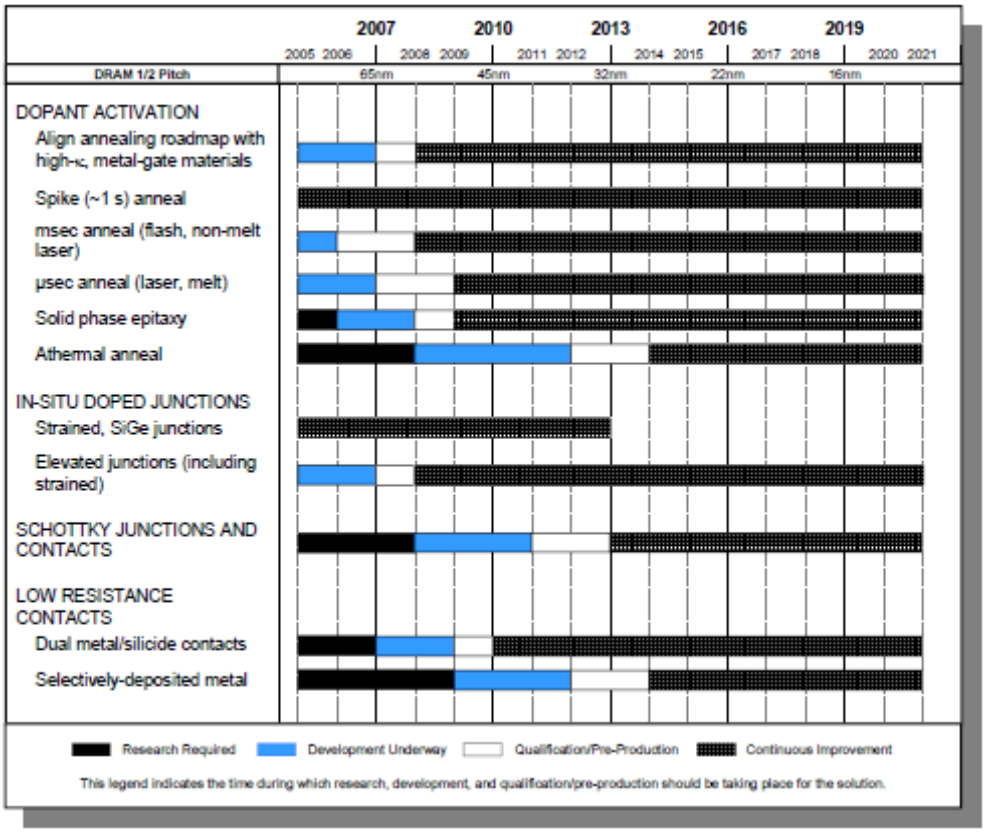

Fig3. Doping Potential Solutions

1.1.2 Characteristic of Plasma Doping Method

In these year, as rapidly downsizing, conventional ion implantation technology is too difficult to control low energy implantation for ultra-shallow junction formation. Plasma Doping has characteristic as following.

Low Bias Voltage (0.2-0.5keV)

High Throughput

short Doping time

Another advantage of PD method can be given isotropy and anisotropy. 3-dimention formations such as trench sidewall can be doped.

1.2 Motivations of This Study

This work has two problems of Plasma Doping technique process. One is resist related problems on Plasma Doping method. Second problem is solid phase epitaxial growth on plasma doping method.

1.2.1 Resist Related Problems on Plasma Doping Method

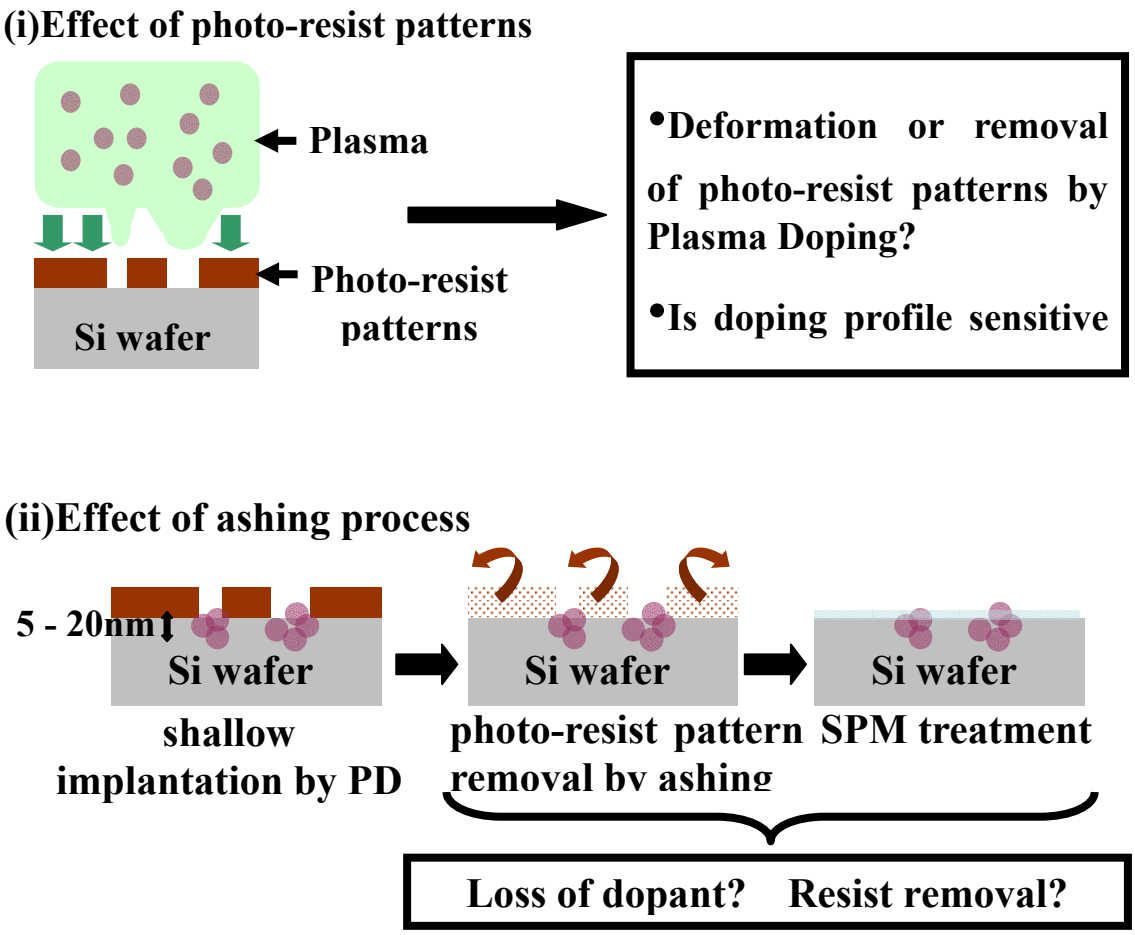

However, in the practical device processes, plasma doping should be carried out with resist patterns in some cases. In this case, the following problems are predicted.That is, these two problems .One is effect of existence of photo-resist patterns on doping properties, and, the other is effect of ashing process which is necessary after the doping process.When the plasma doping is carried out on the wafer with photo-resist patterns, plasma sheath may be deformed due to non-uniform electrostatic condition which is caused by partial charging up of resist patterns and their three dimensional features. Thus we should notice a possibility of dose and doping profile may change depending

on the resist patterns.As well as the effect on the doping properties, effects of plasma on the photo-resist patterns themselves should be considered. That is, deformation of resist patterns by the plasma.After the doping process with resist patterns, we have to remove the resist pattern by ashing process. And after that, we consider use of SPM wet treatment, because we have obtained experimental results that the post SPM treatment was useful to preserve dopant in the substrate even after the activation annealing. In these processes, we suspect that the high density dopants located very near the surface were lost by the ashing process.Therefore we studied these two things through the experiments. The purpose of this work is, to find out whether the photo-resist patterns with various size affect boron dose, and to check the dose loss after the ashing process.

1.2.2 Solid Phase Epitaxial Growth on Plasma Doping Method

Pre-amorphization layer formed by PD has different from that by Ion Implantation. View of a-Si epitaxial growth using annealing, it is important to study on the difference.

1.3 Outline of the Thesis

This thesis is composed of five chapters. In this chapter, we describe Background of this study, PD, tendency on shallow junction cited from ITRS2005.

In chapter2, I descripe farication and measurement methods using my experiments.

In chapter3, We discuss photo resist related problems on PD.

In chapter4, We discuss Solid Phase Epitaxial Growth on PD. Here, I studied eight themes on SPE using PD.

Finally, in chapter5 we describe future issues about PD.

Chapter 2. Fabrication and Measurement Methods

2.1 Experimental Equipment of This Study

2.1.1 Plasma Doping Method

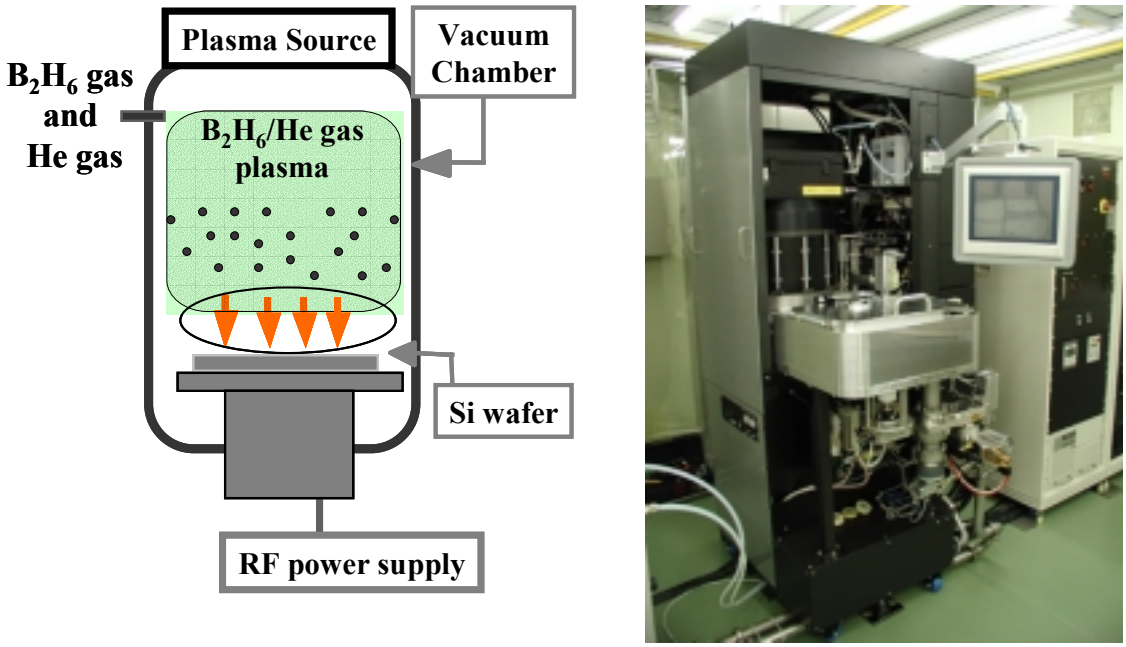

Fig.2.1 Photograph of plasma doping system and schematic diagram illustrating general conception of doping mechanism.

Plasma doping technique is different from ion implantation. Simplification like omitting the intermediate stages of ion source, beam extraction, focusing and scanning, make plasma doping compatible for mass doping. The gas source is immersed in plasma environment into radicals, ions, or neutrals. Charge particles like ions can be accelerated in direction to the target wafer by means of a series of pulsed negative high-voltage.

Photograph of plasma doping system and schematic diagram illustrating general conception of doping mechanism is depicted in Fig. 2.1. Two chambers (i.e., loading chamber and process chamber) and two high voltage RF-power supplies (i.e., for source and for acceleration bias) and Langmuir probe for measuring plasma distribution are utilized in the system. Helicon source give the system to have low-pressure and

high-density plasma source. The process chamber is accommodated with turbo molecular pump with background pressure of 10^{-5} Pa. The doping process is carried out at pressure of 0.9 Pa. Several gases like helium (He) and diborane (B_2H_6) are available to be plasma targets in the process chamber.

2.1.2 Rapid Thermal Annealing

Thermal processes are often used for defects recovery or molecular introduction to dielectric thin films, for lattice recovery or impurity electrical activation of doped or ion implanted wafers. In this experiment, Rapid Thermal Processing MILA-3000 from ULVAC is used for annealing deposited La_2O_3 thin films. Fig. 2.2 illustrated the schematic drawing for MILA-3000. High purity gas ambience can be obtained by pumping out and purging with the in use ambient gas. This RTP system is heated-up by infrared lamp heating furnace and cooled-down by flowing water radiator. The furnace temperature is of the range from room temperature to around 1200^{o}C with ramp-up of less than 50^{o}C/sec and much slower on cooling-down. The available of ambient gases are N_2 and O_2 at atmospheric pressure by keeping the flowing gas at the rate of 1 lt./min.

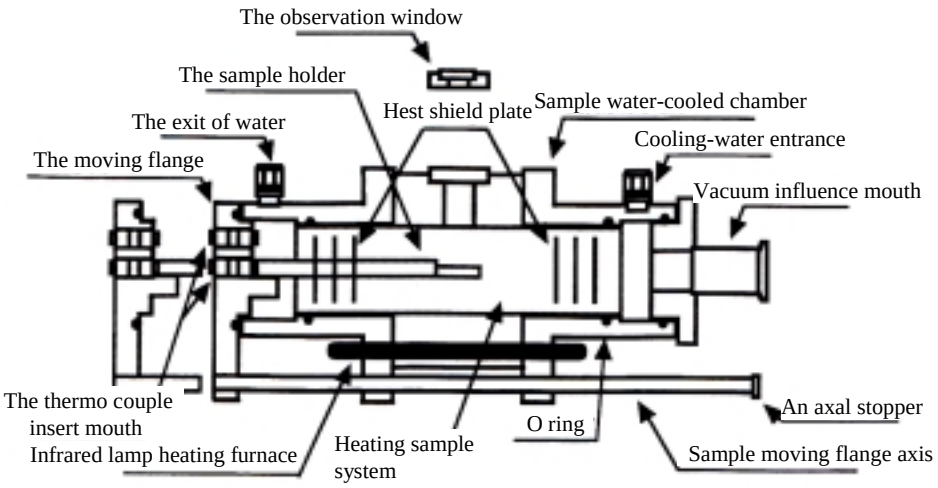

Fig. 2.2Schematic drawing for Rapid Thermal Annealing (RTA) MILA-3000. High

purity gas ambience can be obtained by pumping out and ambient gas purging.

2.1.3 Vacuum Thermal Evaporation Method

All of Al metals in this work were obtained from deposition with bell jar vacuum thermal evaporation. Fig. 2.3.1 illustrates a schematic drawing for vacuum thermal evaporation system. The system is utilized with Turbo Molecular Pump (TMP) to pump down to several 10^{-5} Torr. In case of MIS capacitor fabrication, metal shadow mask with circle opening of 100 μm and 200 μm diameters was used. Filament is made of tungsten, was used for heating the Al source up to its vapor temperature. Both filaments and Al sources are made of Nilaco, inc. with material purity of 99.999%.

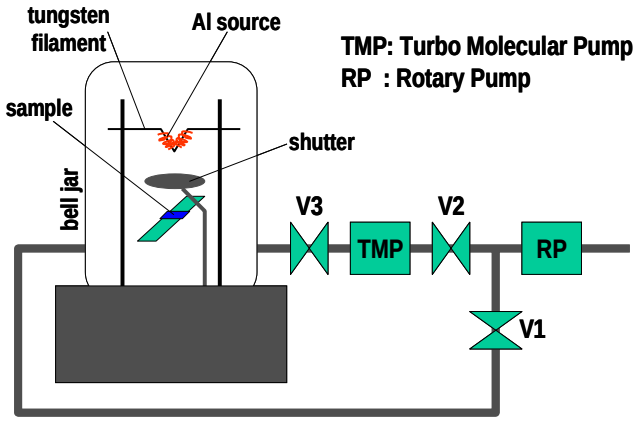

Fig. 2.3.1 Schematic drawing for vacuum thermal evaporation system. The system is utilized with Turbo Molecular Pump (TMP) to pump down to several 10^{-5} Torr.

The physics of vacuum thermal evaporation is based on thermodynamics of the evaporated materials. There have been experiments performed for evaluating the

thermodynamic properties of material. Careful evaluation may reveal that the vapor pressure of liquid Al is given by the following.

$$\log P_{torr} = \frac{15{,}993}{T} + 12.409 - 0.999 \log T - 3.52 \times 10^{-6} T \qquad \textbf{Eq. 2.1}$$

Neglecting the last two terms, the Arrhenius character of log P vs. 1/T can be essentially preserved. Fig. 2.3.2 presents thermal equilibrium for metal evaporations in form of Arrhenius plots. The dot marks are the metal melting points. Two modes of evaporation can be distinguished in practice, depending whether the vapor effectively emanates from liquid or solid source. Usually, a melt will be required if the element in question does not achieve a vapor pressure greater than 10^{-3} torr at its melting point. Most metals, like Al, Ag, Au, and so on, fall into this category, and effective film deposition is attained only when the source is heated into the liquid phase. On the other hand, elements such as Cr, Ti, Mo, Fe, and Si reach sufficiently high vapor pressures of 10^{-2} torr some 500^{o}C below the melting point.

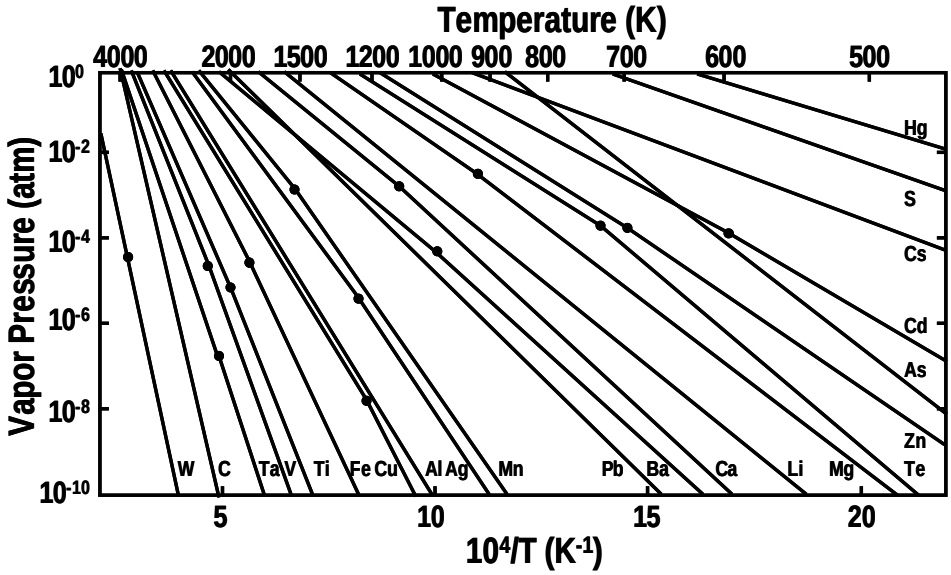

Fig. 2.2.2 Thermal equilibrium for metal evaporations in form of Arrhenius plots. The dot marks are the metal melting points.

2.2 Measurement Method

2.2.1 Secondary Ion Mass Spectroscopy(SIMS)

Fig. 2.2.1 shows measurement for analyzing element compositions, depth profiles, and surface properties with Secondary Ion Mass Spectroscopy (SIMS). This technique is limited to element detection and capable for analyzing most of elements, isotopes or molecular species. As shown in the figure, the basically SIMS measurement is destructive. It is bombarding the sample with primary ions (i.e., Ar^+, O_2^+, Cs^+, and so on), the sputtered secondary ions are detected with energy analyzed and separated with mass spectrometer.

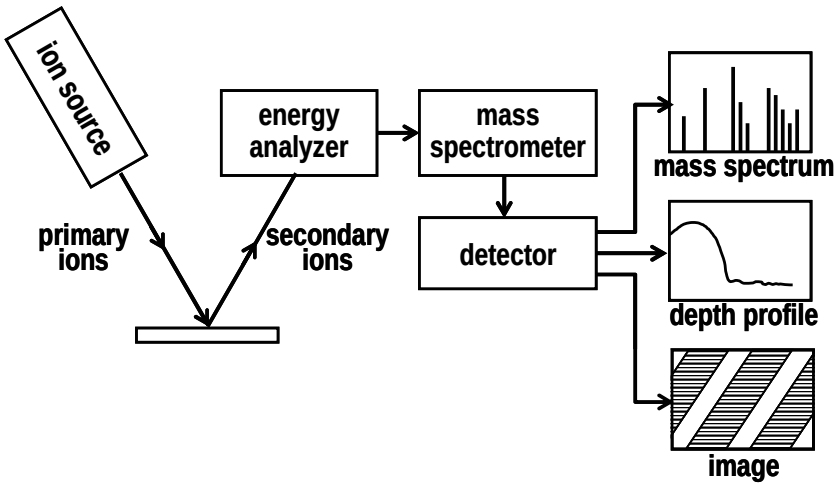

Fig. 2.2.1 Measurement for analyzing element compositions, depth profiles, surface properties with Secondary Ion Mass Spectroscopy (SIMS).

2.2.2 Spectroscopic Ellipsometry

Ellipsometry is the method to estimate the optical property of material or surface film thickness the change of polarization condition caused by the reflection of light. Generally, when light is illuminated to a material, the polarization condition of incident light and reflected light are different. This method evaluates the surface condition from this difference. P component of polarized light is horizontal to the plane formed by incident and reflected light and vertical component is S. Ordinary non-polarized light becomes linear polarized light in which the phase and intensity are the same between P and S polarization component when it was passed through 45^o declined polarizer. When the linear polarized light is illuminated to the material, phase different Δ arises between P and S component of polarized light because the reflectance of P and S component is different at the material surface(Fig.2.2.2)

P and S component in electric field vector of the reflected light are given by

$$\begin{aligned} E_P &= a_P \cos(\omega t - \delta_P) \\ E_S &= a_S \cos(\omega t - \delta_S) \end{aligned} \qquad (1)$$

Here, a_P, a_S are amplitudes of P and S direction respectively. δ_P and δ_S express the phase deviations in the each component. Introducing the relation $\delta_P + \delta_S = \Delta$, the following equation is obtained.

$$\frac{E_P^2}{a_P^2} + \frac{E_S^2}{a_S^2} - 2\frac{E_P E_S}{a_P a_S}\cos\Delta = \sin^2\Delta \qquad (2)$$

This equation expresses ellipsometry in general. The condition of elliptically polarized light is determined by the relative phase difference Δ and reflection amplitude ratio. Taking the tangent, reflection amplitude ration is expressed as reflection amplitude angle ψ ellipsometer measures and determines Δ and ψ or $\cos\Delta$ and $\tan\psi$.

Following system is assumed for the typical measurement. The system consists of

ambient, thin film, and substrate.

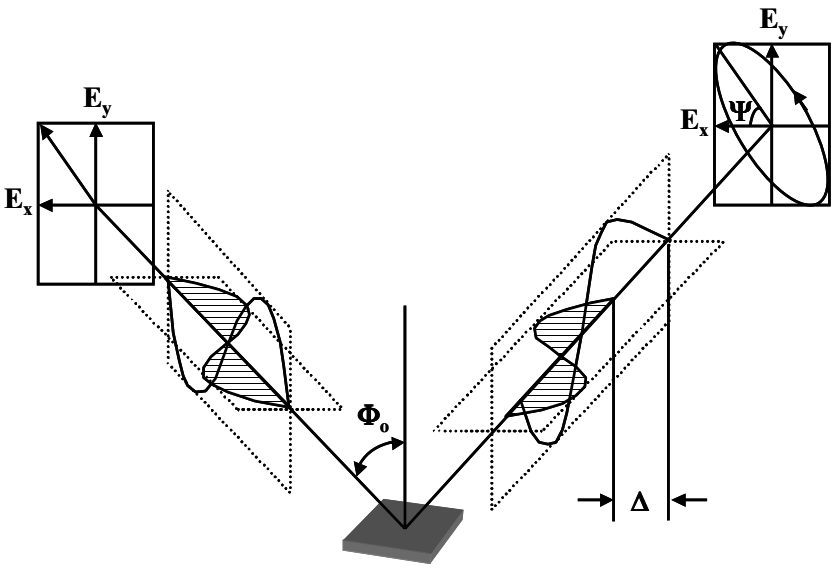

Fig.2. Conception for measuring optical thickness of thin film with spectroscopic ellipsometry.

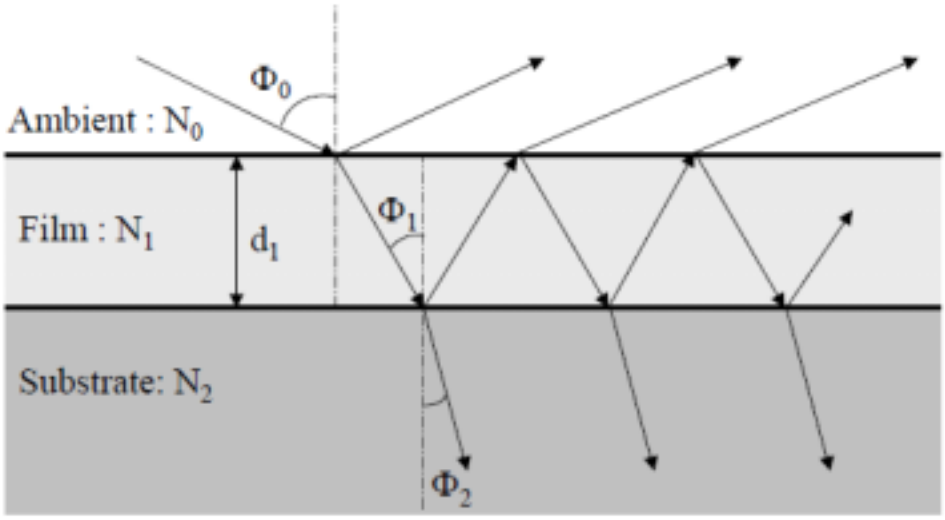

Fig.2 model of typical thin film measurement

The relation between reflectance ratio in P, S component of polarized light and ellipsometry parameter is expressed as

$$\tan\psi e^{j\Delta} = \frac{R_P}{R_S} \qquad (2.3)$$

Here, R_P and R_S are complex reflection constant(Fresnel constant). Giving complex refraction $N_i = n_i - jk_i$, Fresnel constant at each interface is given by

$$r_{i,j+1} = \frac{N_i \cos\Phi_{i-1} - N_{i-1} \cos\Phi_i}{N_i \cos\Phi_{i-1} + N_{i-1} \cos\Phi_i}$$
$$r_{i,j+1} = \frac{N_{i+1} \cos\Phi_{i-1} - N_i \cos\Phi_i}{N_{i-1} \cos\Phi_{i-1} + N_i \cos\Phi_i} \quad (4)$$

The phase angle β_i in the i layer film is

$$\beta_i = 2\pi\left(\frac{d_i}{\lambda}\right) N_i \cos\Phi_i \quad (5)$$

Here d_i is film thickness, λ is wavelength of incident light and φ_i is incident angle in the i layer. Using these parameter,

$$R_P = \frac{r_{o1P} + r_{12P} e^{-j2\beta_1}}{1 + r_{o1P} r_{12P} e^{-j2\beta_1}}$$
$$R_S = \frac{r_{o1S} + r_{12S} e^{-j2\beta_1}}{1 + r_{o1S} r_{12S} e^{-j2\beta_{1i}}} \quad (6)$$

Therefore, if complex reflection in each layer, incident angle and wavelength of light at measurement are known, film thickness can be calculated by measuring ellipsometry parameters.

2.2.3 Scanning Electron Microscope(SEM)

The Scanning Electron Microscope (SEM) is a microscope that uses electrons rather than light to form an image. There are many advantages to using the SEM instead of a light microscope.

The SEM has a large depth of field, which allows a large amount of the sample to be in focus at one time. The SEM also produces images of high resolution, which means that closely spaced features can be examined at a high magnification. Preparation of the samples is relatively easy since most SEMs require the sample to be conductive. The combination of higher magnification, larger depth of focus, greater resolution, and ease of sample observation makes the SEM one of the most heavily used instruments in research areas today.

The SEM uses electrons instead of light to form an image. A beam of electrons is

produced at the top of the microscope by heating of a metallic filament. The electron beam follows a vertical path through the column of the microscope. It makes its way through electromagnetic lenses which focus and direct the beam down towards the sample. Once it hits the sample, other electrons (backscattered or secondary) are ejected from the sample. Detectors collect the secondary or backscattered electrons, and convert them to a signal that is sent to a viewing screen similiar to the one in an ordinary television, producing an image.

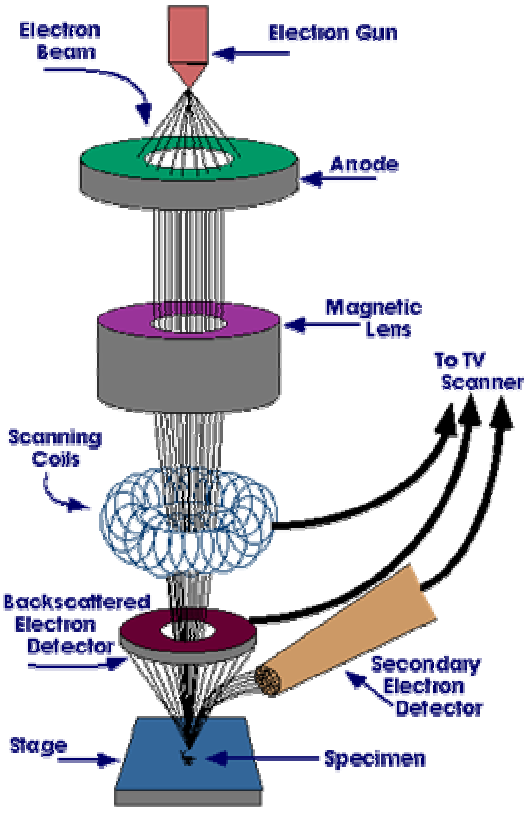

Fig.2.2.3 schematic of SEM

2.2.4 Transmission Electron Microscope(TEM)

Cross-sectional TEM (Transmission Electron Microscopy) is often used to observe the physical thickness or the thin film's morphology. It is compatible for observing nano regime structure, as image resolution as high as 0.2-0.3 nm can be reached by TEM. Fig.

3.9 illustrates schematic diagram for TEM observation. The principle is pretty similar to optical microscope since several magnetic lenses are used to magnify the object image. To penetrate the electron beam, sample as thin as 5-500 nm is. Interaction of electron beam with atomic arrangement in sample may produce interference pattern in transmitted electron beam. High-resolution image can be obtained from imaging the magnified transmitted electron beam.

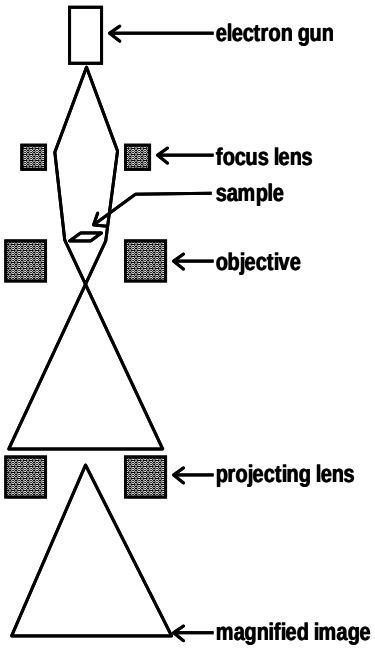

Fig. 2.2.4 A schematic diagram for TEM (Transmission Electron Microscopy) observation. Several magnetic lenses are used to magnify the object image.

2.2.5 Four Point Probe Method

In ultra-shallow junction, formation of shallower junction depth with lower sheet resistance is the main obstacle. There are many ways on measuring sheet resistance of a layer range from permanent contact, temporary contact to contactless techniques. For a semiconductor with resistivity ρ, the resistivity is defined by

$$\rho = \frac{1}{q\left(n\mu_n + p\mu_p\right)}$$

where n and p are the free electron and hole concentrations, and μ_n and μ_p are the electron and the hole mobilities, respectively. The sheet resistance is defined by

$$R_s = \frac{\rho}{t}$$

where t is the layer thickness. The simplest way on measuring sheet resistance is by two-point probe (2pp) method. However, this technique is suffering from the contact resistance R_c at each metal probe/material contact and from the spreading resistance R_{sp} under each probe. Hence, it is difficult to obtain the correct sheet resistance value with two-point probe.

The contact resistance R_c and spreading resistance R_{sp} can be eliminated with four-point probe (4pp) method. Fig. 2.2.5.1 shows schematic drawing for sheet resistance measurement with four point probes. The spaces among the probes are 1 mm. The photograph of four-point probe instrument is given in Fig. 2.2.5.2 An appropriate weight of 50 ~ 150 grams are used to make punch through to the native oxides. This technique assumes that the sample is infinite in lateral area. For finite sample, geometrical correction factor must be applied to obtain the correct result. Fig. 2.2.5.3 depicts the correction factor for measurement of resistivity using four-point probe.

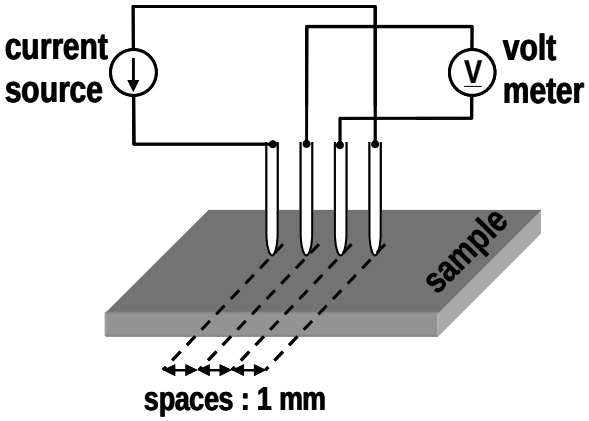

Fig. 2.2.5.1 Schematic drawing for sheet resistance measurement with four point

probes. Spaces among the probes are 1 mm.

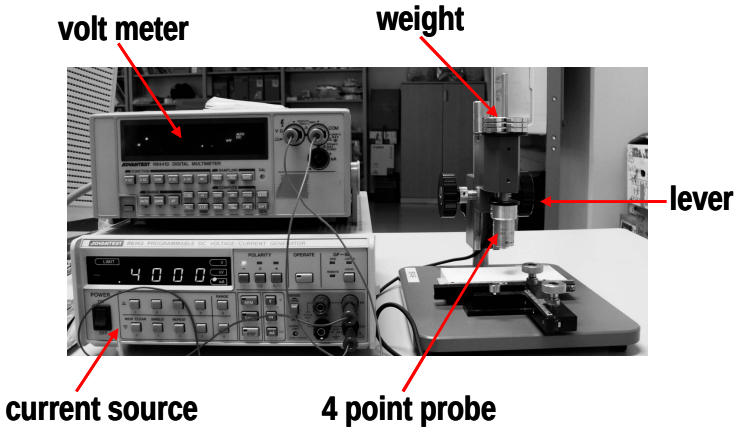

Fig. 2.2.5.2 Photograph of four-point probe instrument. An appropriate weight of 50 ~ 150 grams are used to make punch through to the native oxides.

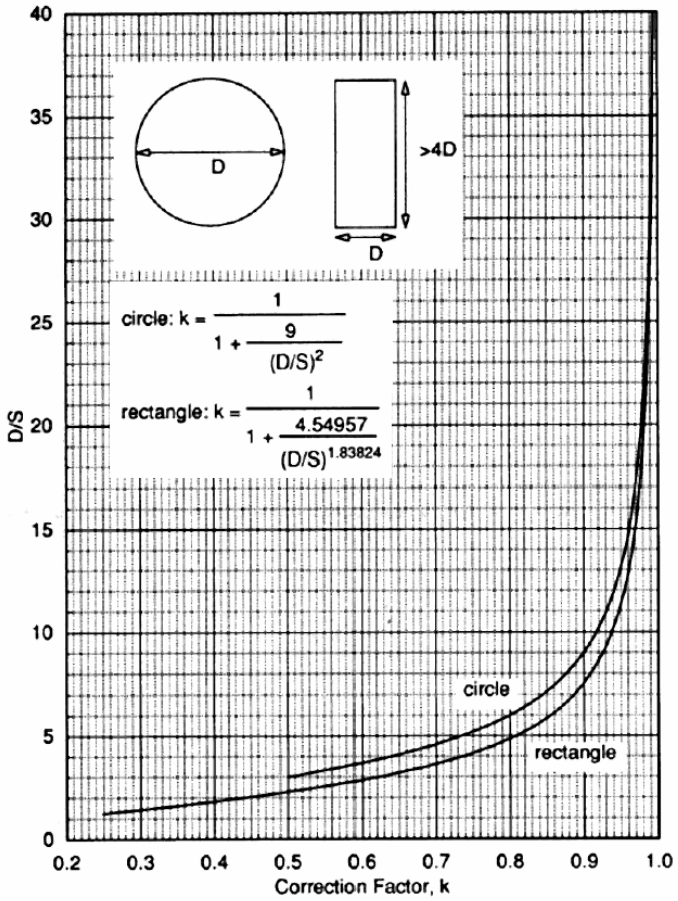

Fig. 2.2.5.3 Correction factor for measurement of resistivity using four-point probe.

2.2.6 Van der Pauw

In order to determine both the relaxation time (mean free path) and the carrier density (Fermi parameters), a combination of a resistivity measurement and a Hall measurement is needed. We discuss here the van der Pauw technique which, due to its convenience, is widely used in research and industry to determine the resistivity of uniform samples. As originally devised by van der Pauw, one uses an arbitrarily shaped (but simply connected, i.e., no holes or nonconducting islands or inclusions), thin-plate sample containing four very small contacts placed on the periphery (preferably in the corners) of the plate. A schematic of a rectangular van der Pauw configuration is shown in Fig. 2.

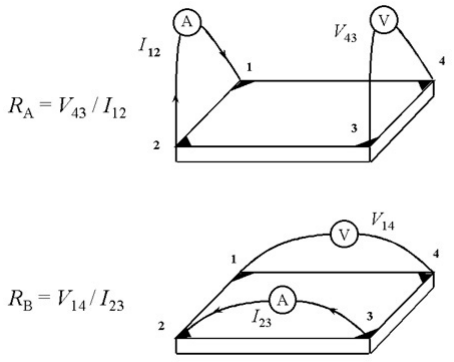

Figure 2

The objective of the resistivity measurement is to determine the sheet resistance R_S. Van der Pauw demonstrated that there are actually two characteristic resistances R_A and R_B, associated with the corresponding terminals shown in Fig. 2. R_A and R_B are related to the sheet resistance R_A through the van der Pauw equation

$$\exp(-\pi R_A / R_S) + \exp(-\pi R_B / R_S) = 1$$

which can be solved numerically for R_S. The bulk electrical resistivity can be calculated using $\rho = R_S d$.

To obtain the two characteristic resistances, one applies a dc current I into contact 1

and out of contact 2 and measures the voltage V_{43} from contact 4 to contact 3 as shown in Fig. 2. Next, one applies the current I into contact 2 and out of contact 3 while measuring the voltage V_{14} from contact 1 to contact 4. R_A and R_B are then

$$R_A = V_{43}/I_{12};\ R_B = V_{14}/I_{23}.$$

The objective of the Hall measurement in the van der Pauw technique is to determine the sheet carrier density n_S by measuring the Hall voltage V_H. The Hall voltage measurement consists of a series of voltage measurements with a constant current I and a constant magnetic field B applied perpendicular to the plane of the sample. Conveniently, the same sample, shown again in Fig. 3, can also be used for the Hall measurement.

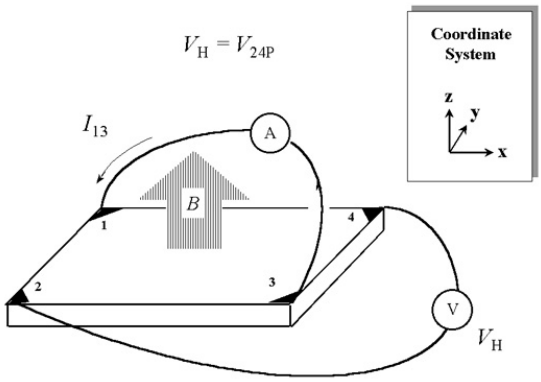

Figure 3

To measure the Hall voltage, a current is forced through the opposing pair of contacts 1 and 3 and the Hall voltage V_H (V_{24}) is measured across the remaining pair of contacts 2 and 4. Once the Hall voltage is acquired, the sheet carrier density can be calculated via

$$n_S = \frac{IB}{e\,|\,V_H\,|}.$$

The bulk carrier density is then $n = n_S / d$.

2.2.7 X-Ray Photoelectron Spectroscopy(XPS)

XPS, which known as Electron spectroscopy for chemical analysis(ESCA) is one of the conventional methods that estimates thin film and Si interface.

Fig.2.2.7 shows photograph and scheme of XPS equipment used in this work. During analysis, the pressures of main chamber were about 10^{-9}(torr) vacuum with turbo pomp. Surface analysis by XPS is accomplished by irradiating a sample with soft X-ray and analyzing the energy of the detected electron. Non-monochromatic MgKα (1253.6eV) X-ray is used in this study. The method is illustrated with the energy band diagram in Fig.2. This photoelectron has limited penetrating power in a solid on the order of 1-10 μm. They interact with atoms in the surface region, causing electrons to be emitted by the photoelectric effect. The emitted electrons have measured kinetic energies given by

$$KE = h\nu - BE - \Phi_S$$

where $h\nu$ is the energy of the photoelectron, BE is the binding energy of the atomic orbital from which the electron originates and Φ_S is the spectrometer work function (4.8eV).

The binding energy may be regatded as the energy difference between the initial and final states of the ion from each atom, there is a corresponding variety of kinetic energies of the emitted electron. Because each element has a unique set of binding energies, XPS can be used to identify and determine the concentration of the elements in the surface. Variation in the elemental binding energies(chemical shift) arises from difference in the chemical potential and polarization of compounds. These chemical shifts can be used to identify the chemical states of the materials being analyzed.

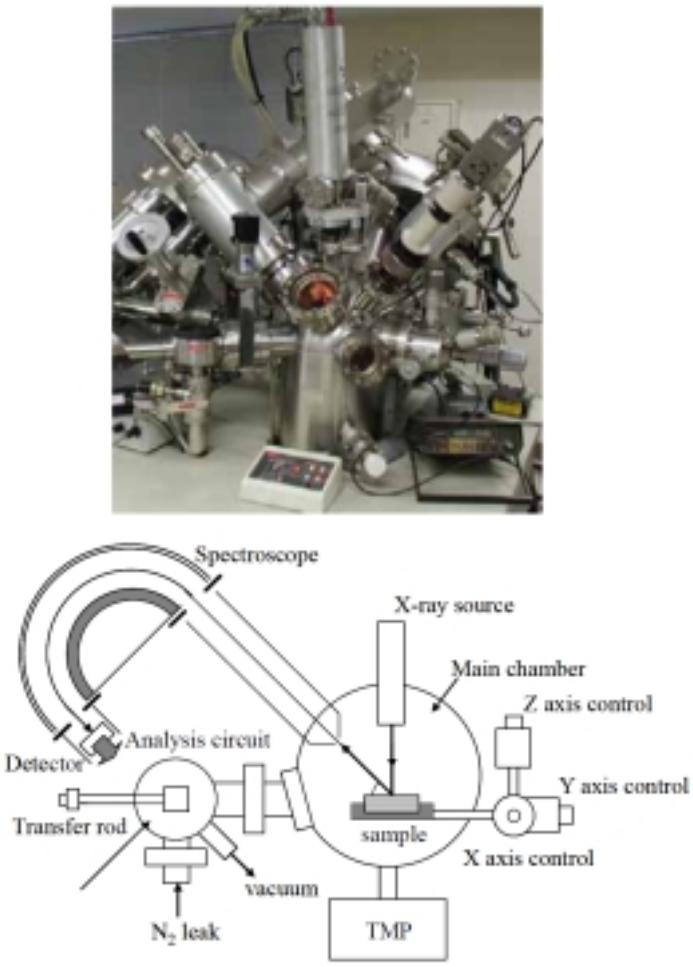

Fig.2.2.7 photograph and scheme of XPS equipment used in this ecperiment

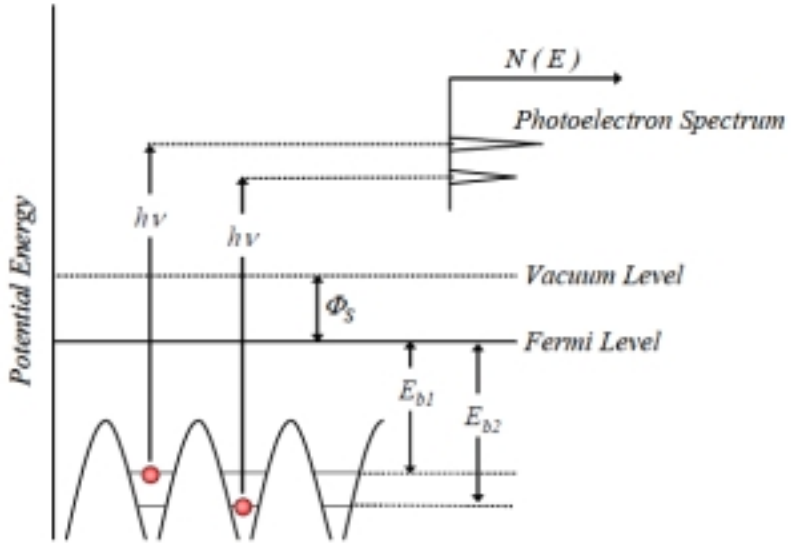

Fig.2 Illustration of measurement method with the energy band diagram

2.3 Wet cleaning

We use wet cleaning during processing in order to prevent contamination of process equipment and to obtain high performance. In this study, sulfuric hydrogen peroxide mixture(SPM H_2SO_4:H_2O_2=4:1), which known as one of RCA cleanings, were performed to remove any organic material ,metallic impurities. And then, native oxide was removed by diluted hydrofluoric acid(HF:H_2O=1:100).

Chapter 3. Resist Related Problems on Plasma Doping Method

3.1 Feasibility Study of Plasma Doping on Si Substrates with Photo-Resist Patterns

3.1.1 Experimental Procedure

Fig.3.1 shows the flow of experiments to see the effect of photo-resist masks on the PD processes. 8-ihch Si wafers with and without photo-resist patterns were prepared, and they were doped with boron by plasma doping. Here, positive type photo-resist whose thickness was about 1 micro meter was used, and patterns were line and space patterns in which size of each region was from 5 to 1000 micro meters.

Then, they are doped by plasma doping, in which a typical doping condition was employed. The source gas was 0.1% B2H6 diluted by He, source power of plasma was 1500W, bias voltage was 60V. Finally, the as-doped boron profiles were measured by SIMS focused on the space regions of the line and space patterns. The measurements were carried out on the L/S patterns from 75/225 micor meters to 300/1000 micro meters and bare wafer as a reference.

(1)The effect of photo-resist patterns

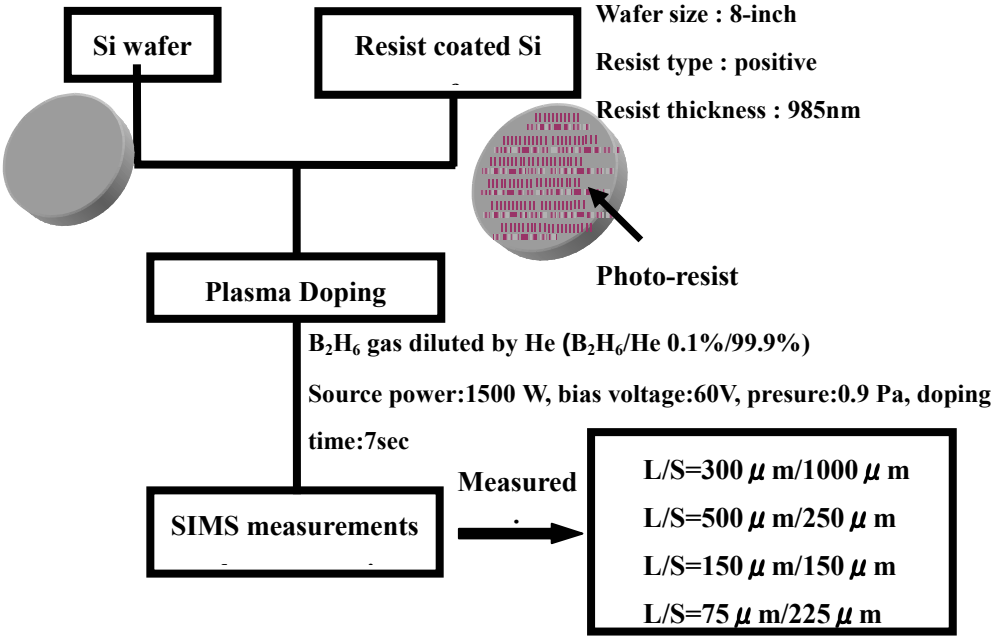

Fig.3.2 shows the flow of second experiment to see the effect of ashing process. At first, the silicon cut-wafer samples doped with boron at four different doses by plasma doping were prepared.The samples were put on a 6-inch wafer and other pieces of wafer coated with photo-resist were placed around the sample as shown in the right figure.Then, they are ashed in o2 plasma, in which a typical condition suitable to removal of 1 micro meter positive photo-resist was employed. The samples processed with the ashing were then treated SPM solution for 10 min. Here, the reference sample which skipped the ashing process was also prepared and treated by SPM at the same time.Finally, They were annealed at 950℃ for 10sec in nitrogen atmosphere and their sheet resistance was measured by four point probe method.

(ii)The effect of ashing process

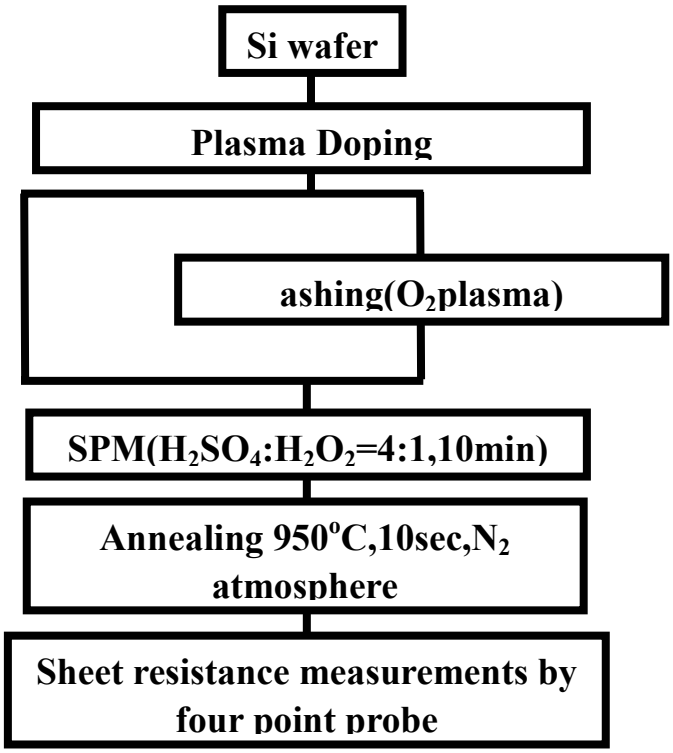

Sample doses

Sample A : 1×10^{15} cm^{-2}

Sample B : 2×10^{15} cm^{-2}

Sample C : 6×10^{15} cm^{-2}

Sample D : 1×10^{16} cm^{-2}

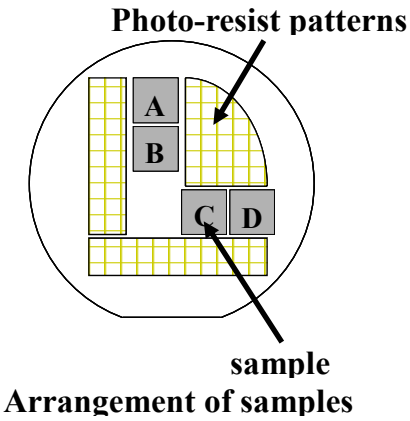

Arrangement of samples

3.2 Experimental Results

3.2.1 The effect of Photo-Resist Patterns

This is the result of the first experiment investigating the effect of resist patterns. The figure shows the SIMS profiles of as-doped boron corresponding to the different size photo-resist patterns.

It was found that all profiles examined here were the same within the experimental error. The average depth of boron at 5x1018cm-3 of these samples was 6.7nm. This result indicates that the presence of photo-resist masks on the wafers did not affect the doping of boron by using the PD in the exposed doping regions.

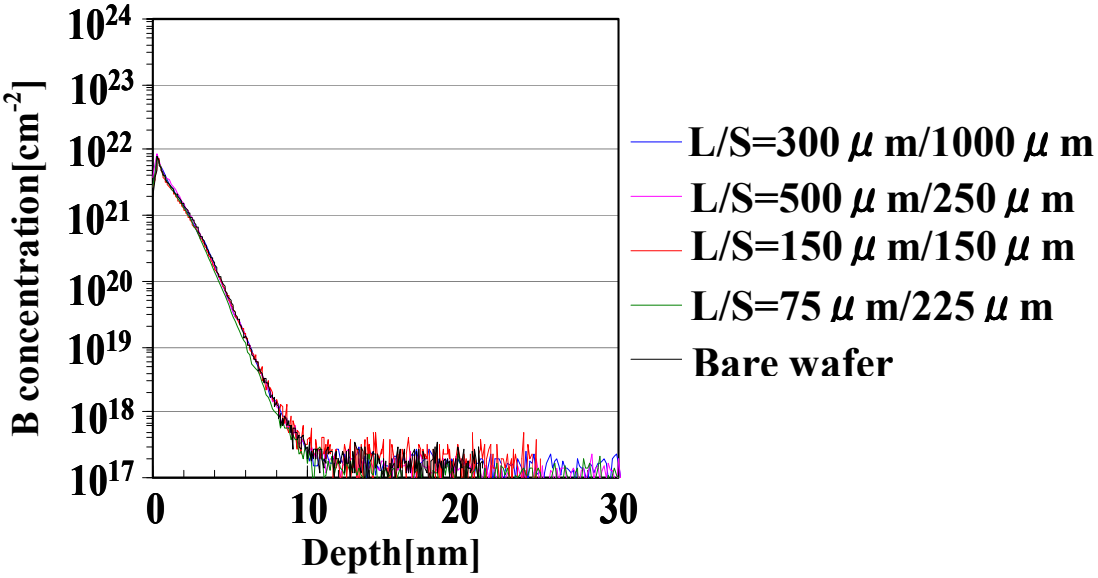

3.2.2 Photo-Resist after PD and Ashing (SEM images)

No deformation of the photo-resist patterns was observed after the Plasma Doping process
The photo-resist patterns were removed completely by the ashing process.

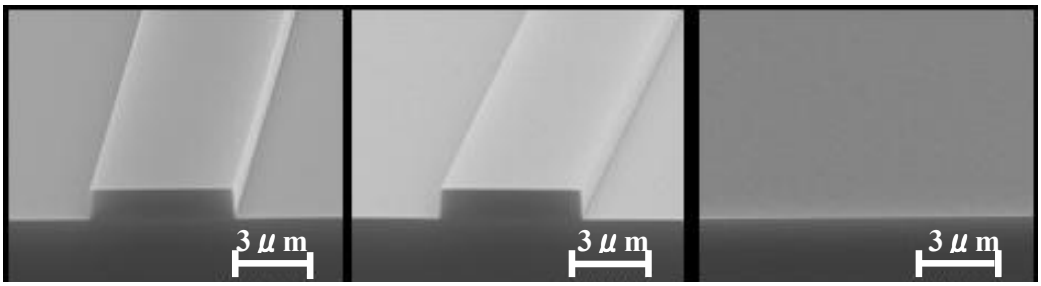

Before Plasma Doping **After Plasma Doping** **After Ashing**

This above figure shows SEM images of photo-resist patterns of line of 5 micro meter width. This is a pattern of the initial state before plasma doping process. And this is after plasma doping. Comparing these two images, notable differences cannot be found. The third image shows an observation after the ashing process, nothing was found on the substrate surface.These observations indicates that deformation of photo-resist patterns by the plasma doping process was not found, and that degradation of the resist was not found at least from the capability of resist removal by O_2 ashing.

3.2.3 The effect of ashing process on dose

The ashing process doesn't affect boron dose, for the dose range from 1×10^{15} to 1×10^{16} cm^{-2}

***Rsash*: *Rs* of samples treated by ashing**
***Rso*: *Rs* of samples not treated by asing**

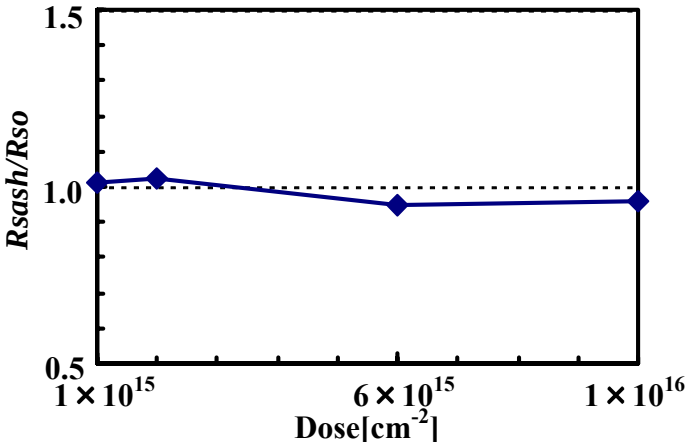

This is the result of the second experiment to see the effect of ashing process on dose of boron after the annealing. The figure shows sheet resistance of the sample treated with ashing process normalized by that without asshing process. That is relative difference of sheet resistance caused by the ashing process. And it is considered that these sheet resistances are proportional to the boron dose after the annealing process in this experiment. Thus, the result that all normalized sheet resistances are very close to unity indicates that the ashing process did not affect boron dose as far as the initial dose was within the experimental condition.

3.2.4 Summary

- It was demonstrated that PD processes were not affected by presence of the photo-resist masks regardless of their line and space patterns examined(150μm-1000μm).
- No deformation of the photo-resist patterns was observed after plasma doping process.
- It was found that the photo-resist patterns were completely removed by the ashing process.
- The ashing process was found not to affect boron dose, for the dose range from 1×10^{15} to $1\times10^{16}cm^{-2}$.

3.3 Photo-resist Removal Using Wet Process after Plasma Doping

Resist removal after plasma doping (PD) by wet process using SPM solution was investigated. Resist patterns exposed to the plasma in the PD process were confirmed to be removed by the SPM treatment although it takes longer time compared to those without plasma exposure. It was also found that the SPM treatment for the as-doped Si surface was preferable to maintain higher retained dose of boron.

3.3.1 Introduction

Plasma Doping (PD) [1-3] is one of the most promising candidates of the impurity doping method to form shallow junctions for 45nm node and beyond it. In practical device processes, PD on wafers with resist patterns is indispensable. Thus, effects of the resist patterns on doping properties, resist removal process and retained dose are significant issues because they should be different from those in the case of conventional ion implantation method. Wet treatments for the resist removal process, instead of conventional ashing process, is worth to be considered relating to the problem of retained dose. We revealed that Sulfuric Acid-hydrogen Peroxide Mixture (SPM) treatment was useful to retain dose of boron after PD [4]. If the SPM treatment can be used for resist removal, it will be desirable process for formation of ultra shallow junction using PD. In this work, condition of resist removal by SPM and retained dose after the SPM process were investigated.

3.3.2 Experimental Procedure

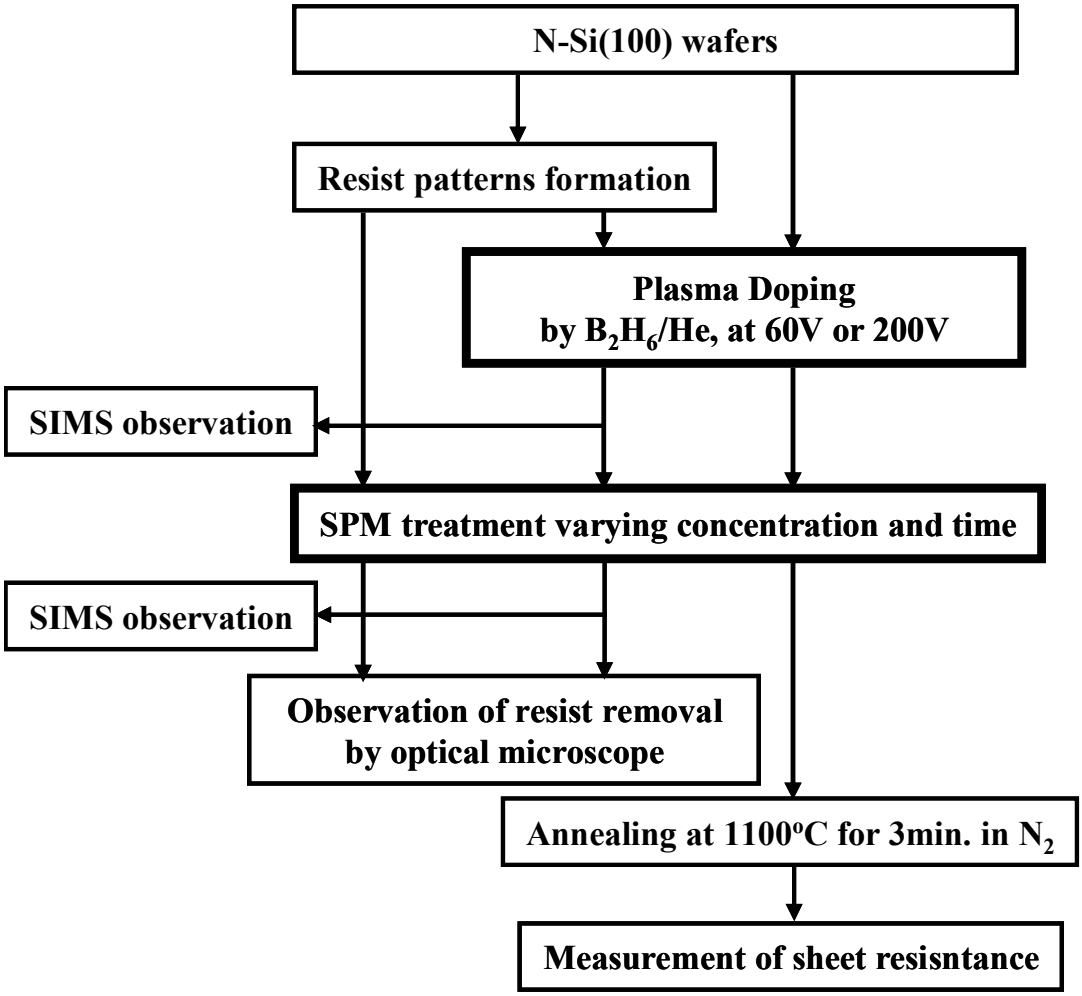

Fig.1 Experimental procedure to study resist removal process and retained dose effects by SPM treatment.

Entire experimental procedure is shown in Fig.1. N typed Si(100) wafers with and without resist patterns were used for substrates. These substrates were doped with boron by the PD method, in which B_2H_6 gas diluted by He was used and bias voltage was 60V or 200V.

The doped wafers with resist patterns, as well as a reference one without PD, were treated by SPM solution (H_2SO_4:H_2O_2=4:1, 3:1, 2:1 or 1:1) at 100^oC varying the treatment time. The treated samples were observed by an optical microscope to find condition of complete removal of the resist patterns. Boron depth profiles were

observed by secondary ion mass spectroscopy (SIMS) before and after the SPM (3:1) treatment.

The wafers without resist patterns doped by the PD process were also treated by SPM (H_2SO_4:H_2O_2=3:1) at 100°C varying the treatment time. The doped substrates before and after the SPM treatment varying treatment time were annealed at 1100°C for 3minutes in N_2 ambient. The annealing was carried out for the purpose of estimating the retained dose of boron from sheet resistance measured by the four-point probe method.

3.3.3 Experimental Results

Table 1 shows time at which resist patterns were completely removed by the SPM treatment, depending on composition of SPM solution and PD conditions. It was found that the resist exposed to plasma could be removed completely by these SPM treatments although it took longer time comparing to the case of non-exposure to the plasma. Dependence of bias voltage was not found in this experiment. The SPM composition of H_2SO_4:H_2O_2=3:1 was found to be optimum from the view point of quick removal of the resist exposed to the plasma.

SPM mixture ratio H_2SO_4 : H_2O_2	Time to remove resist patterns depending on PD conditions		
	No PD	After PD (60V)	After PD (200V)
1:1	75 sec	12 min	15 min
2:1	30 sec	11min	10 min
3:1	60 sec	4 min	4 min
4:1	30 sec	5 min	5 min

Table 1 Treatment time at which resist patterns were completely removed, depending on composition of SPM solution and PD condition.

Figure 2 shows SIMS profiles of boron before and after the SPM treatment (3:1, for 7 minutes), for the bias voltage of 60V. The depth of boron distribution defined at 5 X $10^{18}cm^{-3}$ of 4.5nm, and abruptness of 1.5nm/decade were achieved on these samples. It is noted that the two SIMS profiles were completely the same within the measurement accuracy.

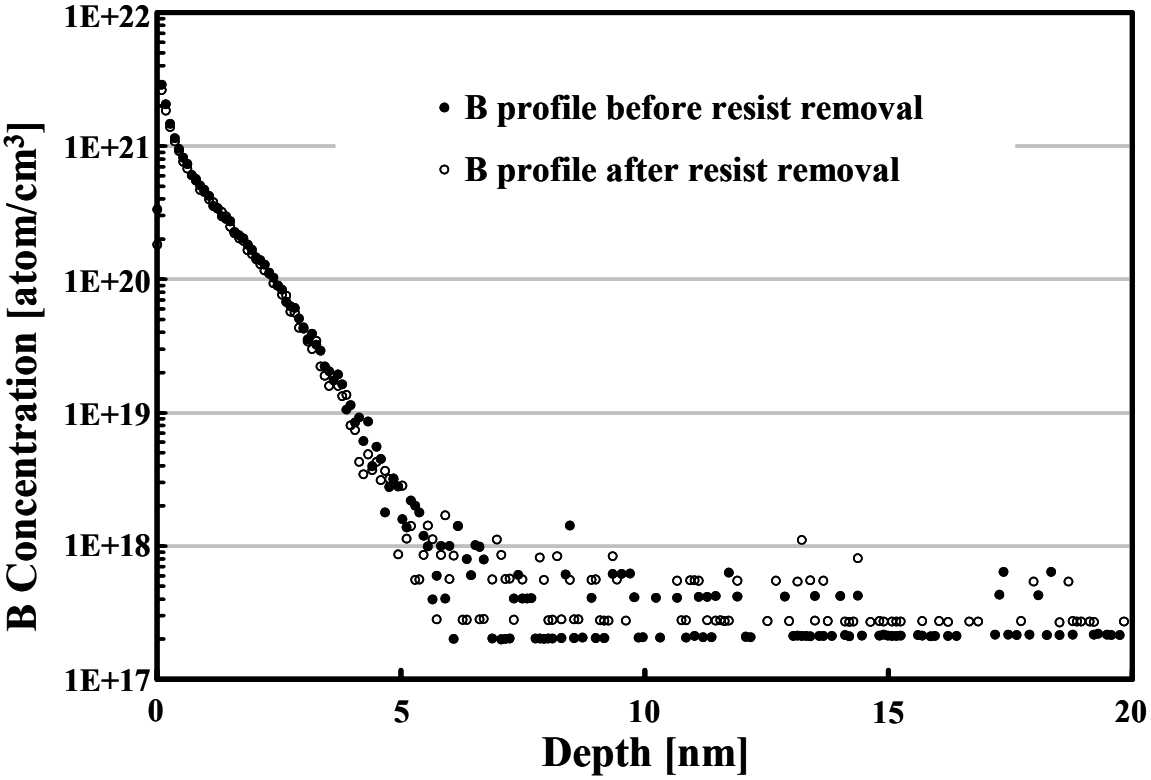

Fig. 2 SIMS depth profile of boron before and after SPM treatment

Fig.3 shows carbon and silicon of SIMS prpfiles before and after SPM treatment. This results indicated that carbon signal was less than silicon signal .

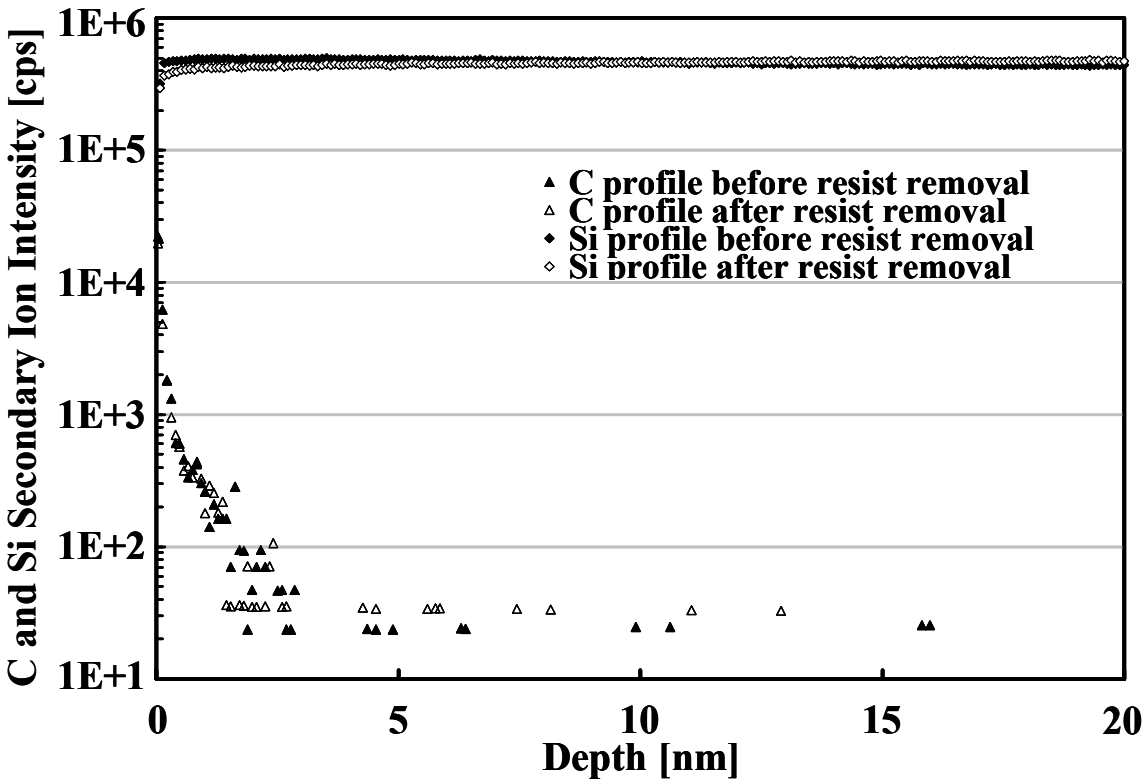

Fig. 3 SIMS depth profile of carbon and Si before and after SPM treatment

Figure 4 shows the change of retained dose of boron after the annealing as a function of the SPM treatment time, in which SPM composition was 3:1. The dose values were estimated from sheet resistances, which was adequate since the annealing condition employed here is considered to be enough for full activation of boron. It was found that the dose for the samples treated by the SPM treatment was larger than that without SPM treatment. This effect was more apparent for the case of bias voltage of 200 V. The experimental results showed that the SPM process can be used for resist removal process without a concern for retained dose, and it is rather preferable from the viewpoint of suppressing the dose loss during the activation process [4].

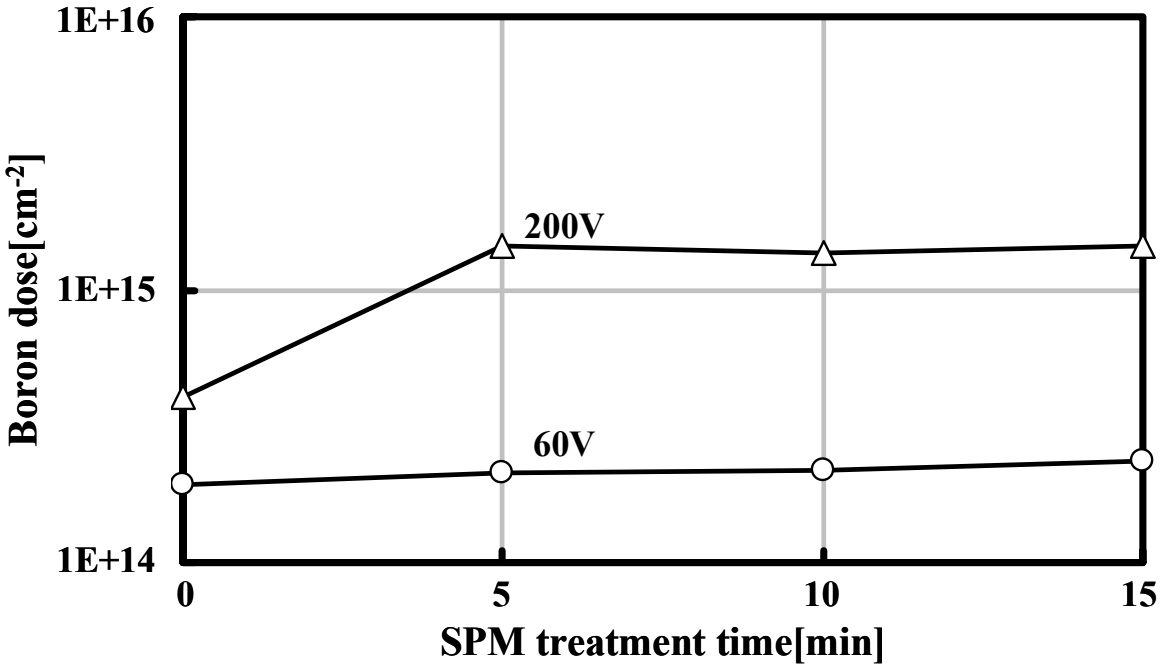

Fig. 4. Dose variation depending on SPM treatment time. Bias voltage in PD: 60V and 200V.

3.3.4 Summary]]

The resist patterns exposed to the plasma were removed completely the SPM treatment, and the preferable properties of retained dose were demonstrated. The resist removal by SPM treatment was fond to be useful for shallow doping process using PD method.

Chapter 4. Solid Phase Epitaxial Growth on Plasma Doping Method

4.1 Introduction

Solid Phase Epitaxial Regrowth (SPE) is considered as a potential method for manufacturing ultra shallow junction for CMOS technology nodes 45nm and smaller. The main advantages are above-equilibrium activation of dopants, minimal diffusion, good control over junction depth, and compatibility with high-k and metal gate thermal budget requirements. The drawbacks of this method are mainly related to the relative high density of residual defects at the end-of range (EOR) region and limited thermal budget for post-anneal processing.

SPE junction formation occurs by low temperature regrowth of an amorphous (a-Si) region containing implanted dopants. For B, a pre-amorphising implant is required. During regrowth, dopant incorporation to substitutional sites is far higher than the equilibrium solid solubility at that temperature for the case of crystalline Si (c-Si). This is likely due to a lower activation energy arising from the lack of a kich-out mechanism as required in c-Si. At such low temperatures (typically 550-650oC) thermal diffusion is negligible with some transient enhanced diffusion (TED) occurring as the point defects diffuse to the surface and bulk. In this thesis I report on how PD and anneal parameters influence Rs and regrowth rate.

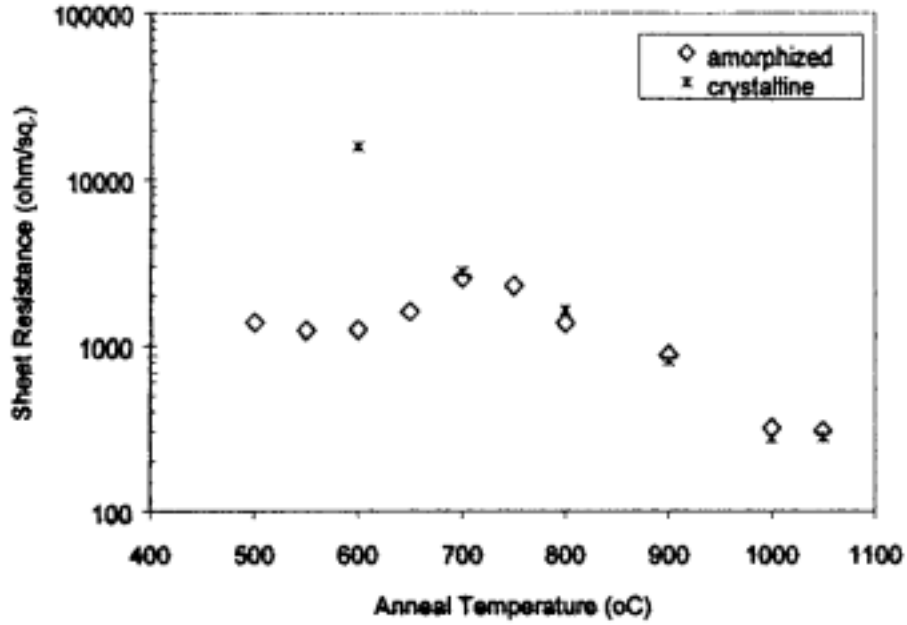

Fig. 1. Sheet resistance of 1keV $1x10^{15}cm^{-2}$ B implant in both crystalline and pre-amorphized wafers, after 30 min anneal at 500°C to 750°C, 60 sec at 800°C, 10 sec at 900°C and 1000°C and spike anneal at 1050°C, all in nitrogen.

4.2 Study on Sheet resistance Rs of SPE on PD

The process flow is showed as follow. N-typed(100) Si substrates is doped boron by PD, annealed at followed conditions, and measured with four point probe method.

Sample Condition for Experiment

B_2H_6 Concentration : 0.025%-0.7%
Annealing time : Variety
Annealing Temperature : 500^o-1100^o

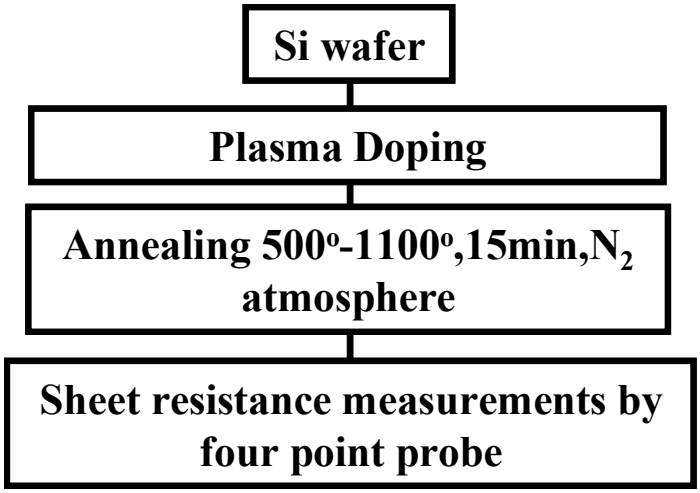

4.2.1 Experimental Results for Rs Using SPE on PD

Below figure shows sheet resistance of shallow junction using PD depending on annealing temperature. This Figure found that sheet resistance increased range 650-750oC as Rs of shallow junction using ion implantation could be seen.

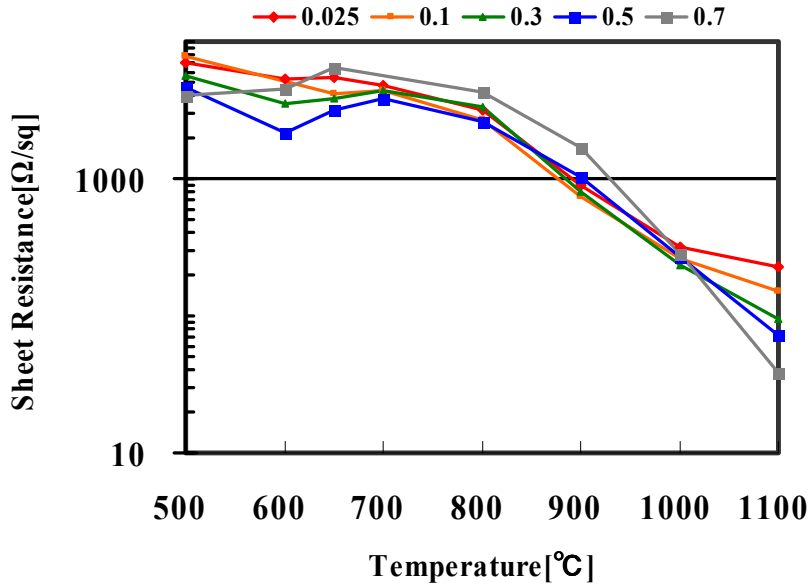

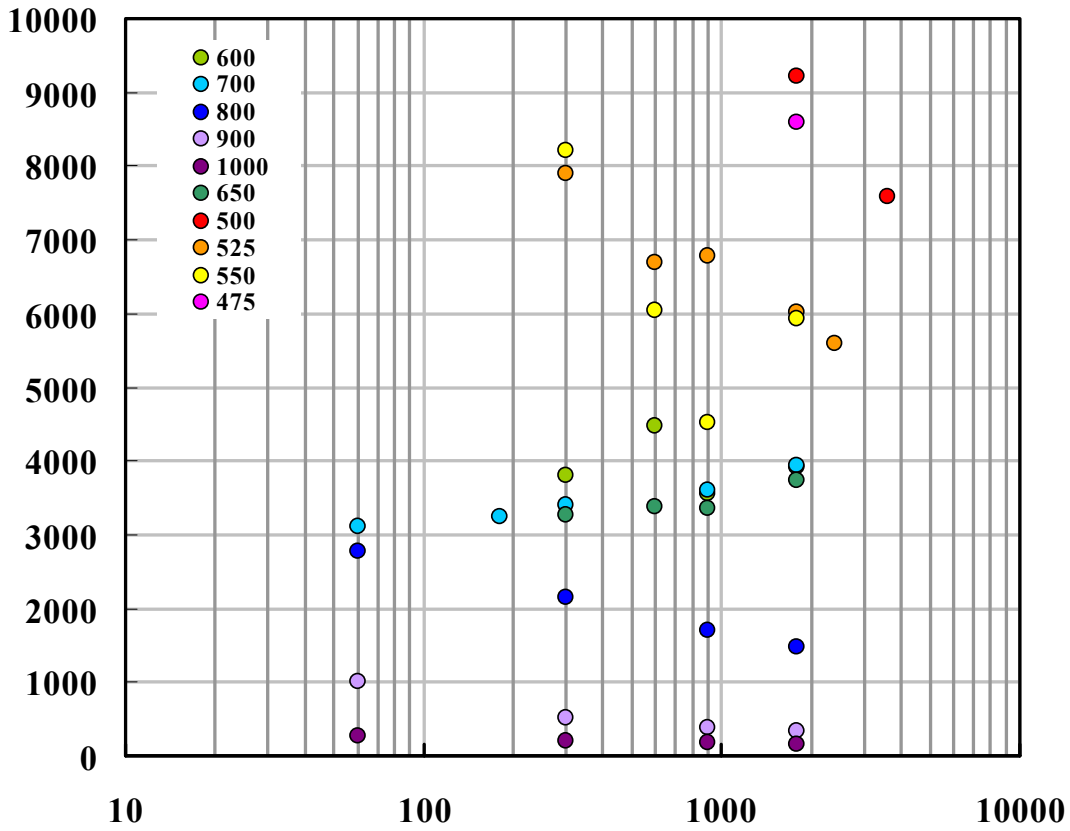
10000
9000
8000
7000
6000
5000
4000
3000
2000
1000
0
10
100
1000
10000
600
700
800
900
1000
650
500
525
550
475

4.3 Dependence on Doping Gas Concentration on SPE

This figure shows results a-Si layer regrowth depending on doping gas concentration using SPE.

This result indicated each condition finished a-Si regrowth at annealing time 15min except 0.7%. but 0.7% remained a-Si layer at several annealing condition.

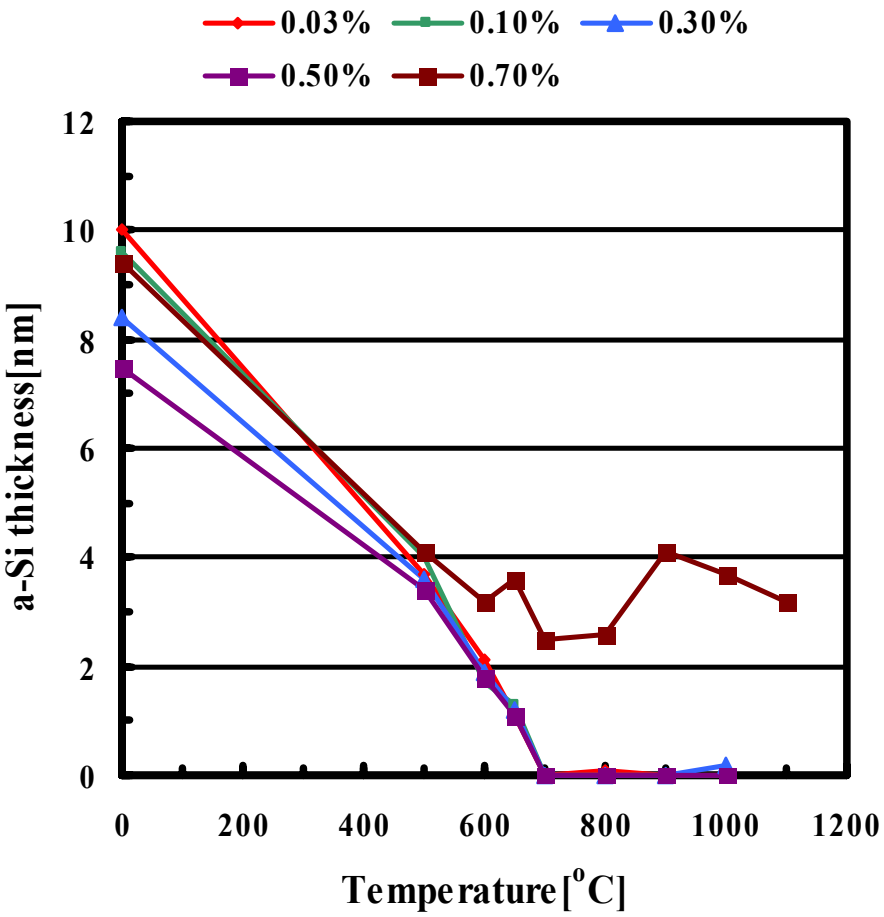

4.4 Rs: Comparison four point probe method and Van der Pauw on SPE

4.4.1 Problem using four point probe method

We anticipated that Rs didn't measure due to punch through shallow junction as like less than 10nm. This reason confirmed the difference Rs measurement of four point probe and van der pauw.

4.4.2 Experimental Procedure

We shows flow process as follow.

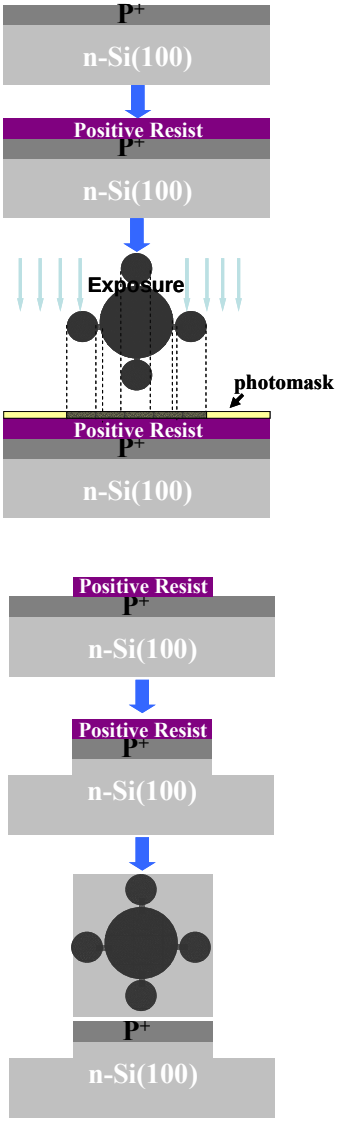

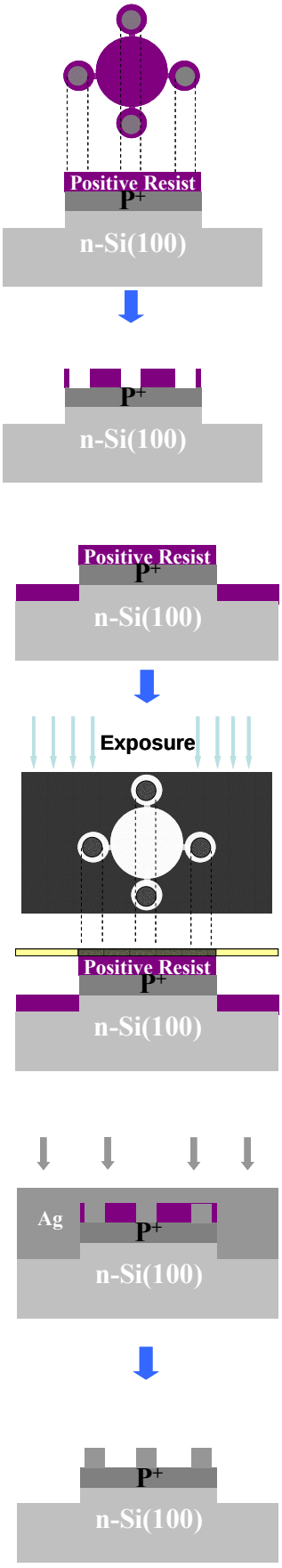
Positive Resist
P+
n-Si(100)
P+
n-Si(100)
Positive Resist
P+
n-Si(100)
Exposure
Positive Resist
P+
n-Si(100)
Ag
P+
n-Si(100)
P+
n-Si(100)

4.4.3 Experimental Results

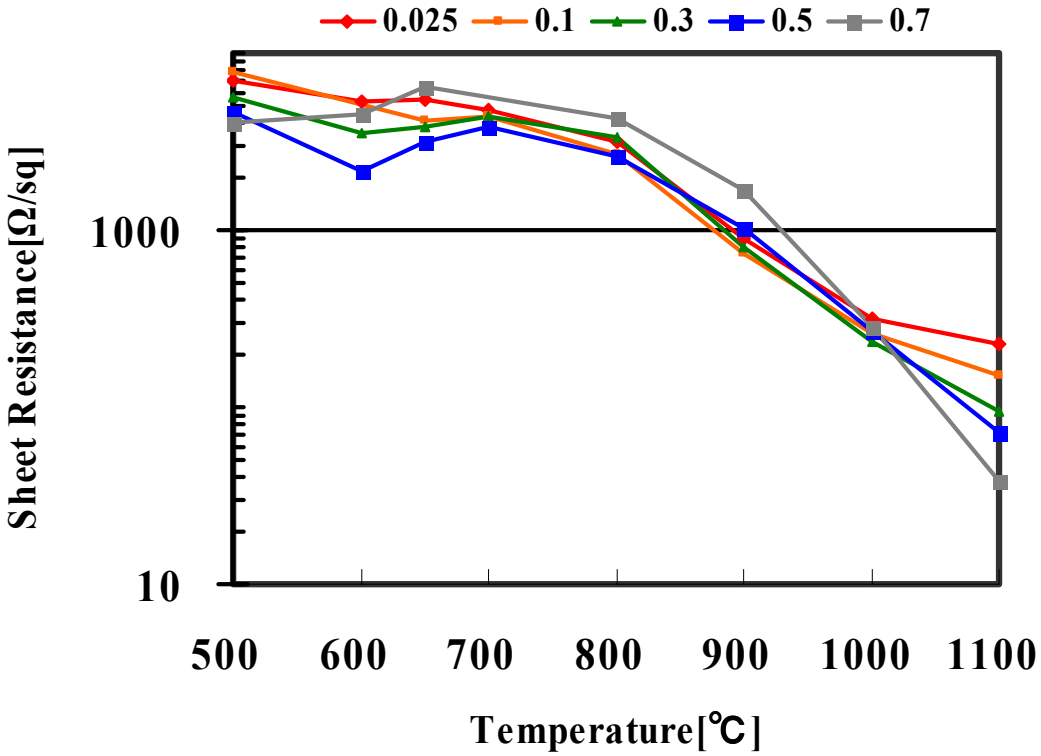

Fig Rs using four point probe. Using Sample is B2H6 concentration from 0.025% to 0.7%

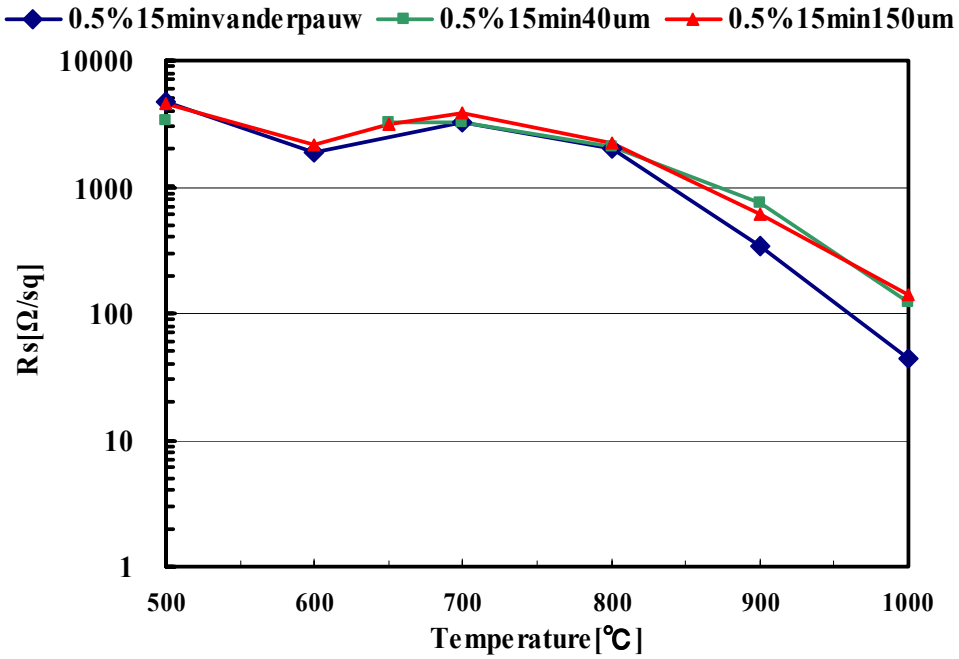

Fig Rs using four Van der Pauw. Using Sample is B2H6 concentration at 0.5%

4.5 Ge-PAI,He-PA,PD の固相成長速度の比較と考察

4.5.1 Background

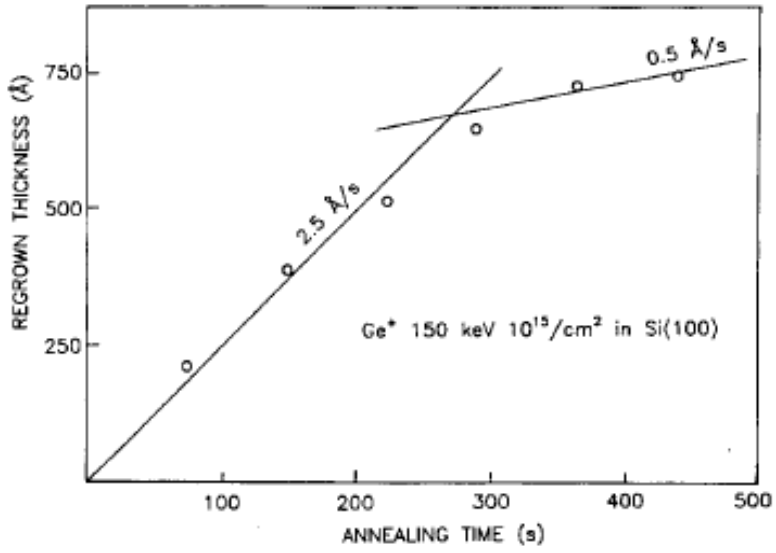

FIG. 4. Regrowth behavior at 525 °C on Ge^+-implanted ⟨100⟩ Si for long annealing times.

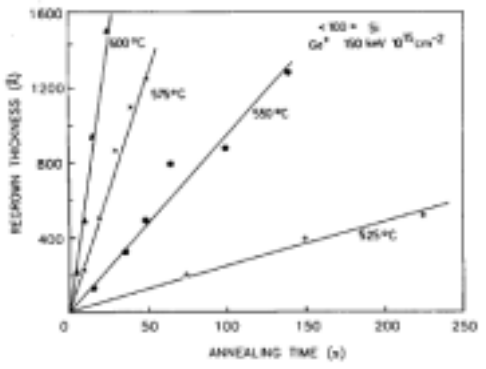

FIG. 1. Regrowth behavior on ⟨100⟩ Si as a function of RTA duration for four temperatures.

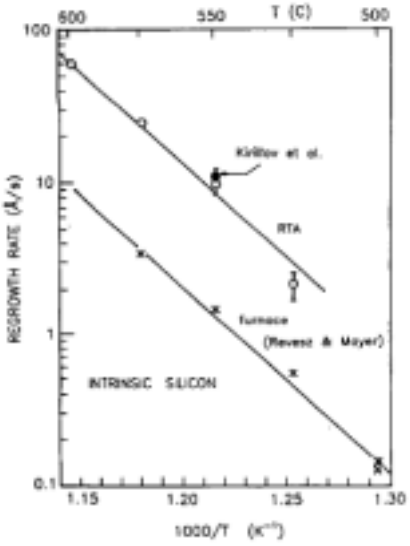

FIG. 2. Regrowth rate vs reciprocal temperature for Ge^+-implanted (intrinsic) ⟨100⟩ silicon. A comparison between furnace annealing (results from Ref. 16) and RTA (our results + 1 point from Ref. 13).

4.5.2 Experiment Result

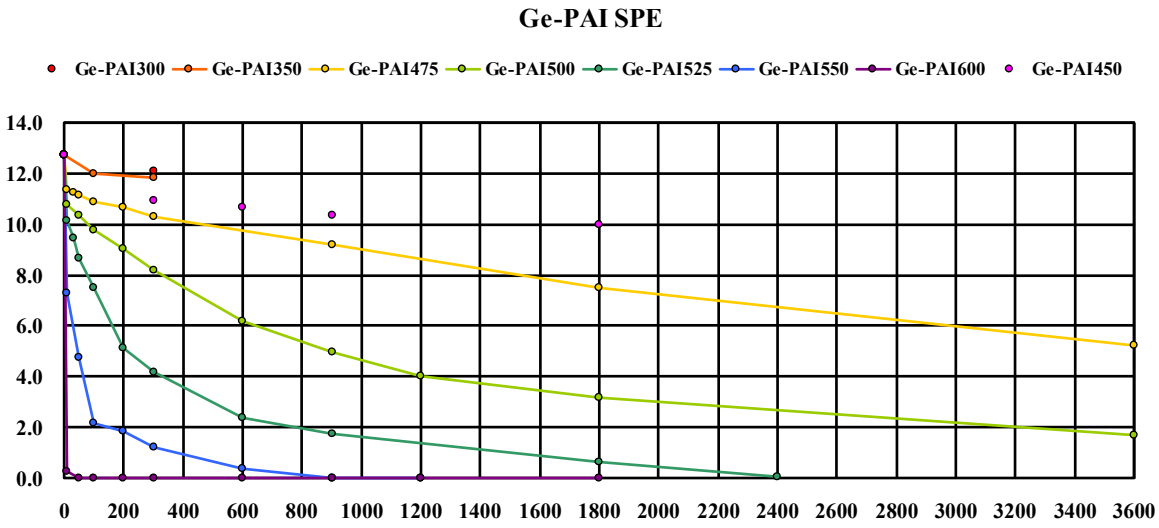

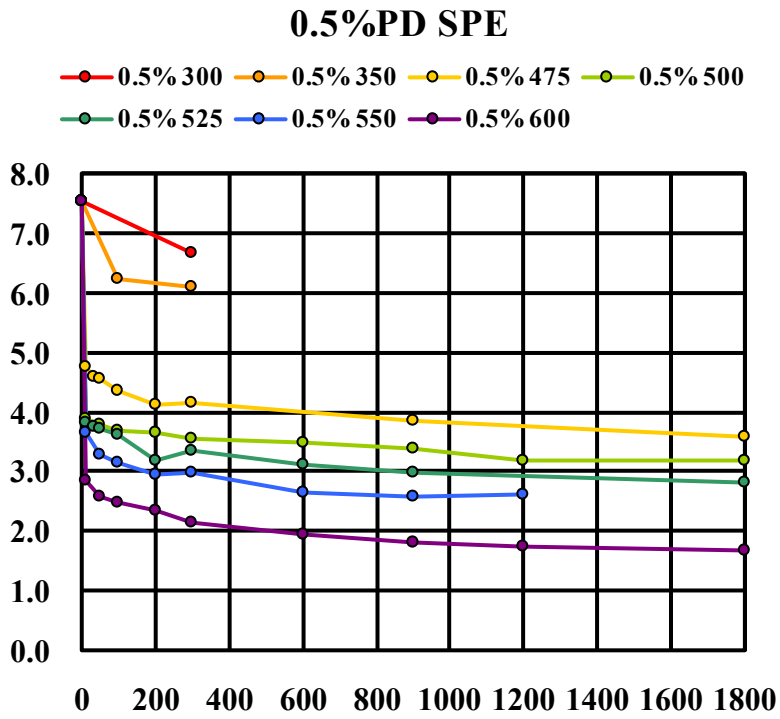

4.6 Boride Confirmation using XPS

4.6.1 Experimental Procedure

This experiment investigated existence boride during annealing process for formation of shallow junction using PD. Below figure shows flow process as follow.

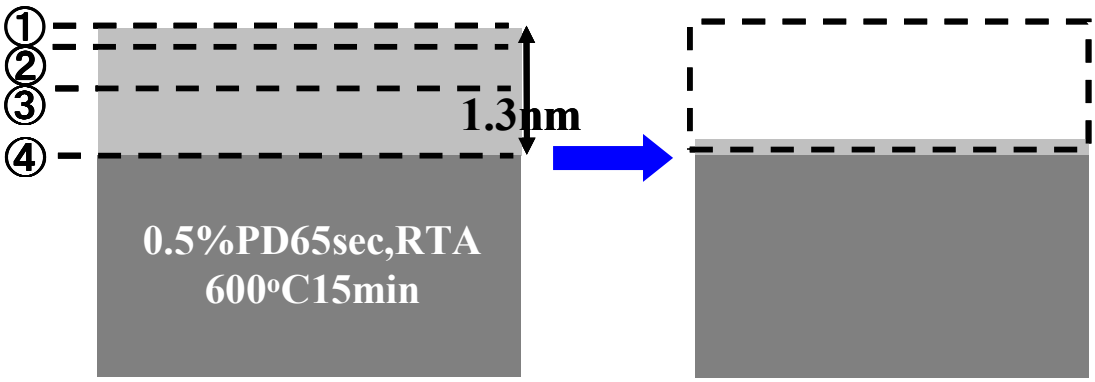

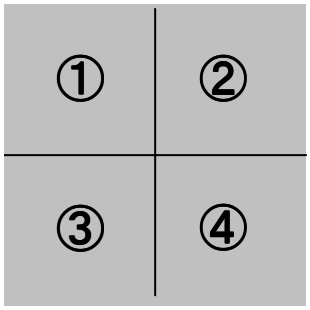

1.surface(Non etching)
2.0.24nmEtching(a-Si layer : 1.1nm)
3.0.7nm etching using 1%diluted HF (a-Si layer : 0.7nm)
4.1.3nm etching 1% diluted HF (a-Si layer : 0nm)

This figure shows etching rate using this experiment.

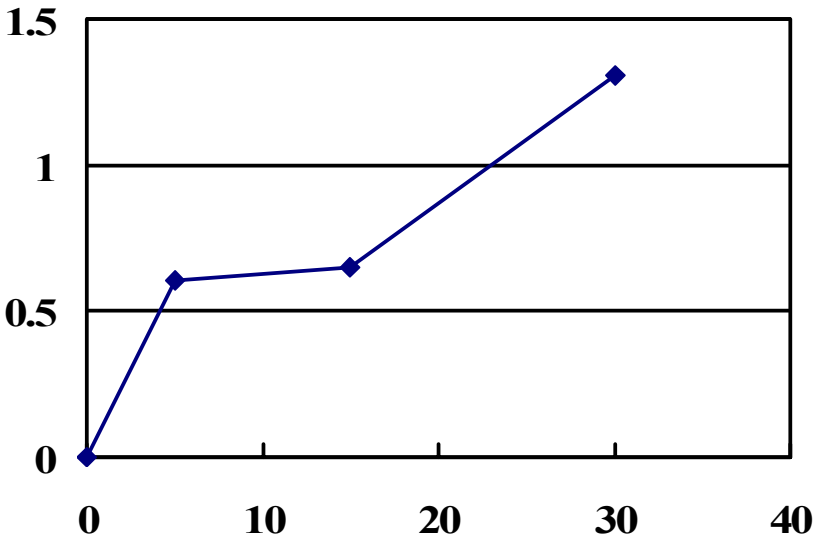

Fig. Etching Rate of 1% diluted HF

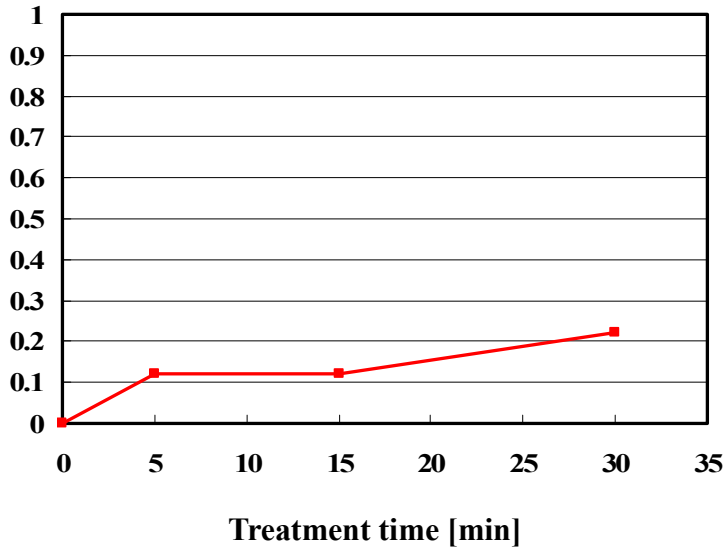

Fig. Etching Rate of NMD3

4.6.2 Experimental Result

This figure shows result obtained from XPS.

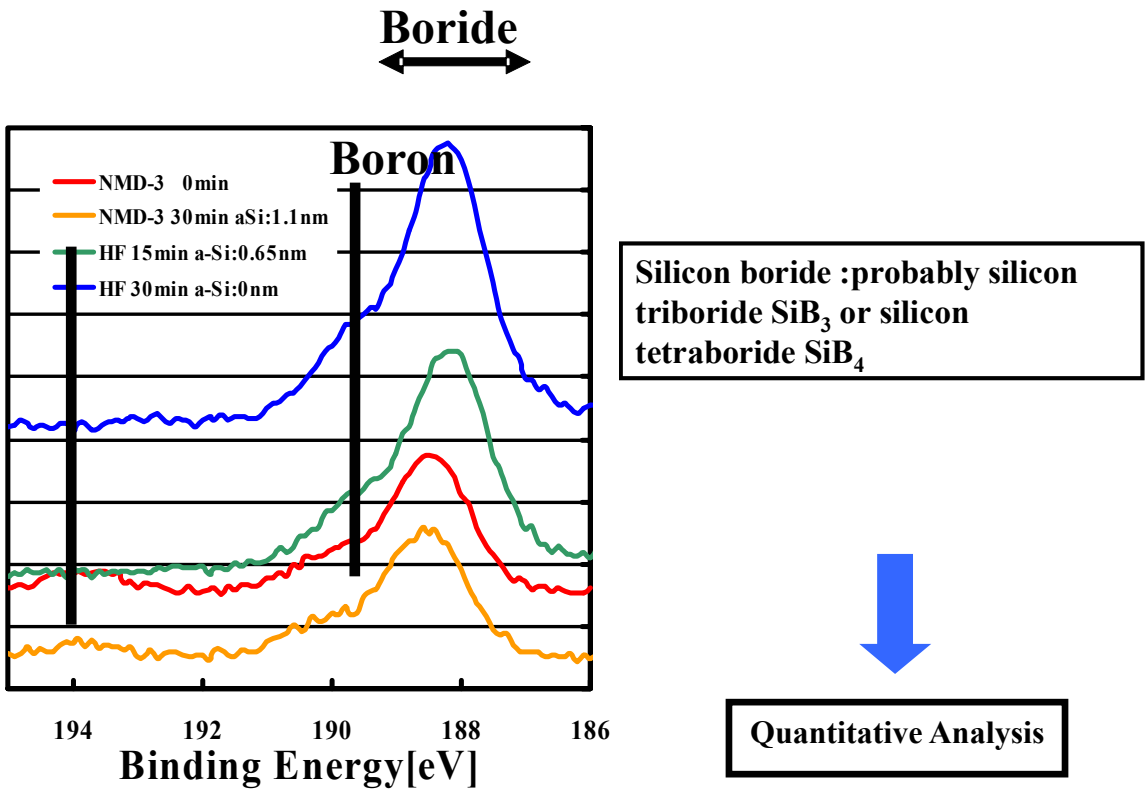

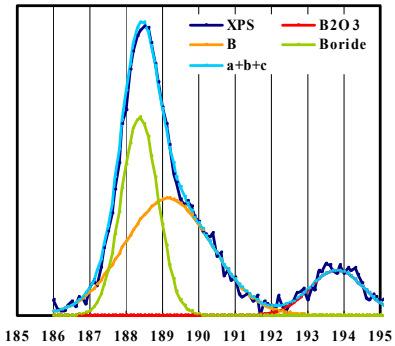

1.表面（エッチングなし）

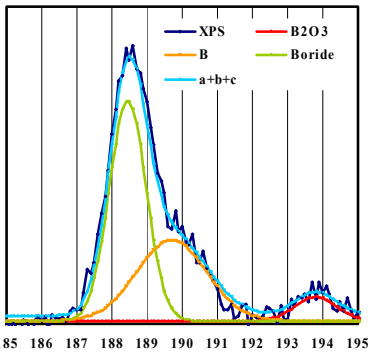

2.0.24nmエッチング(a-Si層：1.1nm)

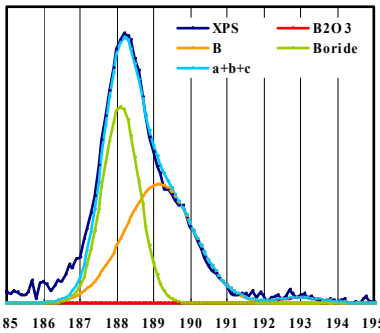

3.0.7nmHFエッチング(a-Si層：0.7nm)

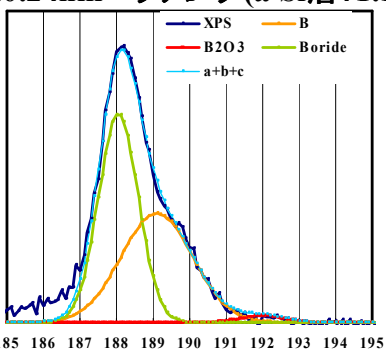

4.1.3nmHFエッチング(a-Si層：0nm)

4.7 Comparison PD and Ge-PAI on Reflection coefficient and absorption cofficient

Ge-PAI と PD は RTA 後にエリプソメーターによる反射係数、吸収係数が違うことがわかった。

以下に考察を記す。

Ge-PAI 後に表面の Si 層が a-Si 層になる。一方、PD（もしくは He-PA）では表面の Si 層が a-Si 層になるが、明らかに反射係数、吸収係数ともイオン注入と違いが見られている。

この結果、アモルファス化された時の反射係数、吸収係数が回復後と同じ PD の場合、RTA による Si 層の回復が I/I に比べて効率がよいため短時間での結晶回復が早いと考えられる。この結果は PD が Flash ramp や spike RTA, Laser Annealing などのナノオーダー、マイクロオーダーの熱照射時間のアニール法に適している可能性が高いことを示していると考えられる。だが、PD は I/I に比べて Si 表面に高濃度にボロンをドーピングまたは堆積してしまうため Si 表面の固相成長速度が急激に遅い傾向がある。

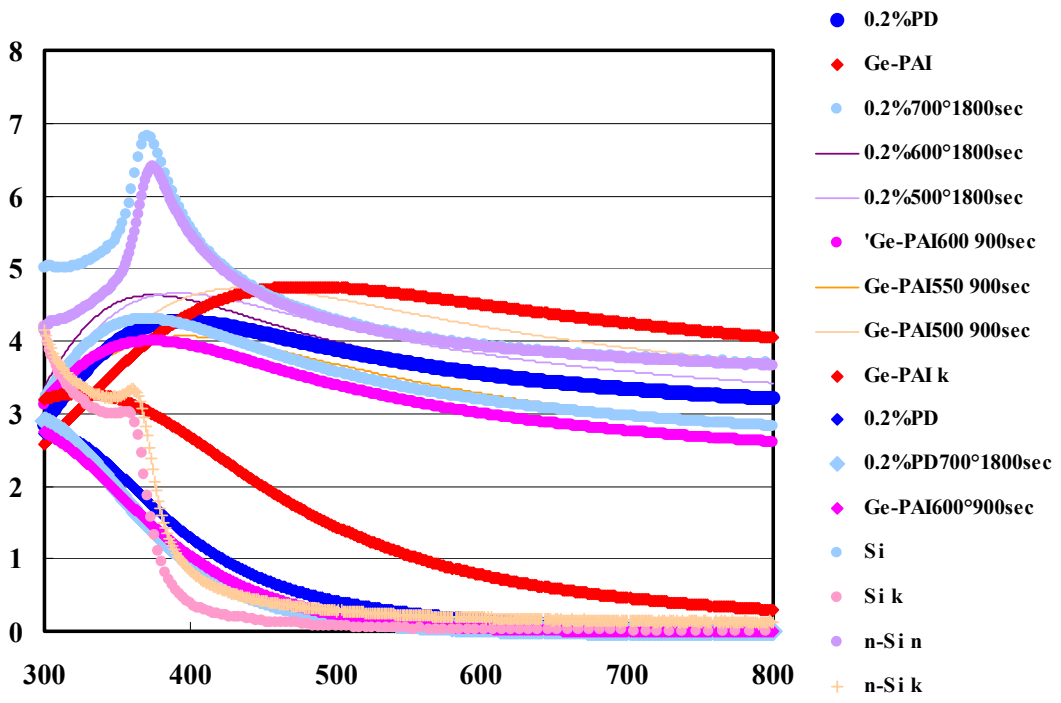
8
7
6
5
4
3
2
1
0
300
400
500
600
700
800
0.2%PD
Ge-PAI
0.2%700°1800sec
0.2%600°1800sec
0.2%500°1800sec
'Ge-PAI600 900sec
Ge-PAI550 900sec
Ge-PAI500 900sec
Ge-PAI k
0.2%PD
0.2%PD700°1800sec
Ge-PAI600°900sec
Si
Si k
n-Si n
n-Si k

4.8 2 Step Annealing Using SPE on PD

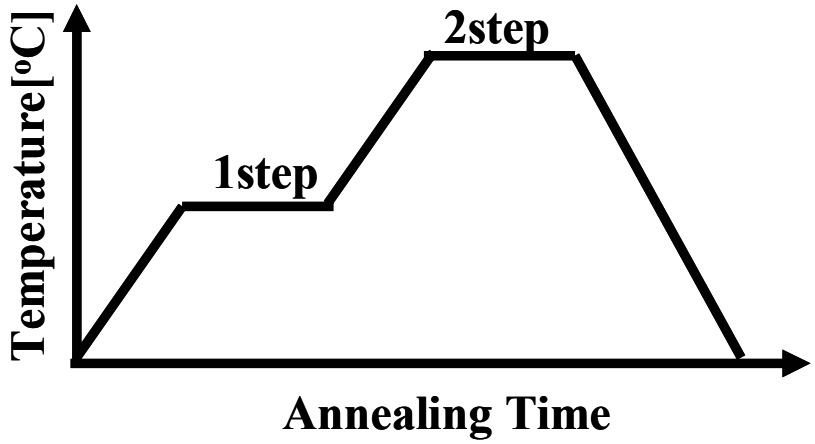

1step		2step		Rs
Temperature[°C]	time[sec]	Temperature[°C]	time[sec]	
0	0	900	60	1014
550	300	900	60	890
550	900	900	60	916
750	60	900	60	896
750	300	900	60	859
750	900	900	60	816

References

[1] Semiconductor Industry Association, et al., “International Technology Roadmap for Semiconductors (ITRS),” 2005.
[2] K. Tsutsui, Electrochem. Soc. Proc., vol. 2004 -01, p.106,2004.
[3] Y. Sasaki, et al …, Symp. on VLSI Tech, p.180, 2004.
[4] T. Sato, et al., 2004 ESSDERC, p.149, 2004

Acknowledgements

This thesis is written under the direction of Professor Hiroshi Iwai, Department of Advanced Applied Electronics, Interdisciplinary of Graduate School of Science and Engineering, Tokyo Institute of Technology. The author would like to express his sincere and deep gratitude to Professor Hiroshi Iwai for his thorough instructions, continuous supports and encouragements.

The author would like to thank to Professor Hiroshi Ishiwara, Professor Kazuya Masu, Associate Professor Kazuo Tsutsui, Associate Professor Eisuke Tokumitsu, Associate Professor Shun-Ichiro Ohmi, Visiting Professor Takeo Hattori, Visiting Professor Nobuyuki Sugii assistant to a professor Kuniyuki Kakushima, and assistant to a professor Parhat Ahmet for their critical comments and valuable discussions.

The author was indebted to Dr. Hiroyuki Ito, Mr. Yuichiro Sasaki, Mr. Cheng-Guo Jin, Mr. Katsumi Okashita, and Hideki Tamura from Ultimate Junction Technology Lab., Inc. for their great supports in researches, facilities as well as valuable discussions. Especially, he would like to express his gratitude to company president Mr. Bunji Mizuno.

The author has spent many days working in laboratory and has found helpful discussion and kind friendship from laboratory fellows. He would like to acknowledge Mr. Yongshik Kim, Mr. Jin-Aun Ng, Mr. Atsushi Kuriyama, Mr. Molina Reyes Joel, Mr. Yoichi Kobayashi, Mr. Takahisa Sato, Mr. Kunihiro Miyauchi, Mr. Hendry anshaer Sauddin, Mr. Kentaro Nakagawa, Mr. Akira Fukuyama, Mr. Yusuke Kuroki, Mr. Satoshi Yoshizaki, Mr. Ruifei Xiang, Mr. Koji Nagahiro, Mr. Song, Mr. Kiichi Tachi, Mr.

Takashi Shiozawa, Mr. Yasuhiro Shiino, Mr. Masayuki Nakagawa, Mr. Chong and Yotaro Fukagawa.

The author would like to appreciate laboratory secretaries, Ms. T. Fukuyama, Ms. N. Iizuka, Ms. A. Matsumoto, and Ms. Y. Hashizume for their supports.

Issui Aiba
Yokohama, February 2006